

1 **Paired electrochemical removal of nitrate and terbuthylazine**  
2 **pesticide from groundwater using mesh electrodes**

3 Roger Oriol<sup>a,1</sup>, Enric Brillas<sup>a,1</sup>, Pere L. Cabot<sup>a,1</sup>, José L. Cortina<sup>b,c</sup>, Ignasi Sirés<sup>a,\*,1</sup>

4 <sup>a</sup> *Laboratori d'Electroquímica dels Materials i del Medi Ambient, Departament de Química Física,*  
5 *Facultat de Química, Universitat de Barcelona, Martí i Franquès 1-11, 08028 Barcelona, Spain*

6 <sup>b</sup> *Chemical Engineering Department, Escola d'Enginyeria de Barcelona Est (EEBE), Universitat*  
7 *Politécnica de Catalunya (UPC)-BarcelonaTECH, Eduard Maristany 10-14, Campus Diagonal-*  
8 *Besòs, 08930 Barcelona, Spain*

9 <sup>c</sup> *Barcelona Research Center for Multiscale Science and Engineering, Campus Diagonal-Besòs,*  
10 *08930 Barcelona, Spain*

11 *Paper submitted to be published in **Electrochimica Acta***

12 \* Corresponding author: Tel.: +34 934039240; fax: +34 934021231.

13 E-mail address: i.sires@ub.edu (I. Sirés)

14 <sup>1</sup>Active ISE member

## 16 **Abstract**

17 Groundwater is one of the main freshwater resources on Earth, but its contamination with  $\text{NO}_3^-$  and  
18 pesticides jeopardizes its viability as a source of drinking water. In this work, a detailed study of  
19 single electro-oxidation (EO) and electrodenitrification and paired EO/electrodenitrification  
20 processes has been undertaken with simulated and actual groundwater matrices containing  $100 \text{ mg}$   
21  $\text{dm}^{-3} \text{NO}_3^-$  and/or  $5 \text{ mg dm}^{-3}$  terbuthylazine pesticide. Galvanostatic electrolyses were made with  $500$   
22  $\text{cm}^3$  of solutions at pH 4.0-10.5 and 250-100 mA in tank reactors with a  $\text{RuO}_2$  or boron-doped  
23 diamond (BDD) anode and one or two Fe cathodes, all of them in the form of meshes. Most of  $\text{NO}_3^-$   
24 removals agreed with a pseudo-first-order kinetics. In  $\text{Cl}^-$ -free media,  $\text{NH}_4^+$  predominated as  
25 electroreduction product. In chloride media, a greater amount of N-volatiles was determined  
26 alongside a slower electrodenitrification, especially with  $\text{RuO}_2$  due to the partial re-oxidation of  
27 electroreduction products like  $\text{NH}_4^+$  by active chlorine. The pesticide decays were also fitted to a  
28 pseudo-first order kinetics, and its presence led to a smaller release of N-volatiles. Overall, BDD  
29 always favored the pesticide degradation thanks to the action of  $\text{BDD}(\cdot\text{OH})$ , whereas  $\text{RuO}_2$  was  
30 preferred for electrodenitrification under some conditions. The EO/electrodenitrification of  
31 groundwater was successful once the matrix was softened to minimize its hardness. The  $\text{NO}_3^-$   
32 concentration was reduced below the limit established by the WHO. Overall, the BDD/Fe cell was  
33 more suitable than the  $\text{RuO}_2/\text{Fe}$  cell because it accelerated the pesticide removal with a simultaneous  
34 high degree  $\text{NO}_3^-$  electroreduction. However, it produced toxic chlorate and perchlorate. A final post-  
35 treatment with an anion exchange resin ensures a significant removal of both ions, thus increasing the  
36 viability of the electrochemical approach to treat this type of water. Chromatographic analyses  
37 revealed the formation of ten heteroaromatic products like desethyl-terbuthylazine and cyanuric acid,  
38 alongside oxalic and oxamic as final short-chain carboxylic acids.

39 *Keywords:* Boron-doped diamond anode; Electrochemical oxidation; Electrodenitrification;  
40 Groundwater; Iron cathode

## 41 **1. Introduction**

42  $\text{NO}_3^-$  ion and pesticides are the main pollutants of groundwater resources in regions with high  
43 density of livestock and agricultural land. The occurrence of these toxic agents is consistently linked  
44 to hazardous health problems and diseases exerted on animals and humans, especially in arid and  
45 isolated regions where groundwater is a direct source for irrigation and drinking water supply [1].  
46 The application of highly effective water treatment technologies is therefore a must in such cases,  
47 aiming to prevent serious health risks. The atmospheric  $\text{N}_x\text{O}_y$  gases, as well as surplus synthetic  
48 nitrogen fertilizers and manure spread on land are the main sources of  $\text{NO}_3^-$  that is further  
49 accumulated in groundwater, attaining contents up to  $900 \text{ mg L}^{-1}$  due to its weak adsorption and high  
50 solubility [1,2]. High contents of this anion may cause methaemoglobinaemia and cardiovascular  
51 illnesses [3,4], and for this reason, the World Health Organization (WHO) limits to  $50 \text{ mg L}^{-1}$  its  
52 concentration in groundwater intended for human consumption. Classical separation methods such  
53 as ion exchange and reverse osmosis are able to remove  $\text{NO}_3^-$  from water [4], but lately more attention  
54 has been drawn to the electrochemical technologies. Among them, electrocoagulation and  
55 electrodialysis have been proven effective as separation methods [5], although there is greater interest  
56 in transformation treatments involving electroreduction. The latter, which is also called  
57 electrodenitrification, consists in the use of an electrocatalytic cathode to increase the activity and/or  
58 selectivity of the  $\text{NO}_3^-$  reduction process. Worth noting, electrodenitrification has been rarely coupled  
59 with electrochemical oxidation (EO) [2,4,5-24].

60 Several factors such as cell configuration, applied current ( $I$ ), solution composition and pH affect  
61 the effectiveness of  $\text{NO}_3^-$  electroreduction. It has been found that this process becomes faster using  
62 electrodes with large overpotential for the  $\text{H}_2$  evolution reaction (HER), owing to the comparatively  
63 slower rate of  $\text{H}^+$  and/or  $\text{H}_2\text{O}$  electroreduction. This has been confirmed from the behavior of metallic  
64 and semiconductor cathode surfaces made of Pd-Rd [6,7], Sn [8,9], Cu [10,11], Cu-Zn [5,12],  
65 stainless steel (SS) [13,14], boron-doped diamond (BDD), SS, graphite, silicon carbide and Pb

66 [15,16], Sn, Bi, Pb, Al, Zn and In [17], Sn modified Pd [18], Fe, Cu, Ni and carbon foams [19], Cu,  
67 Pd, Pt and Rh nanoparticles deposited on reduced graphene [20], Cu-Ni [21], Fe [14,22], TiO<sub>2</sub>  
68 nanotubes [23], and Bi-Pd nanoparticles [24]. The electroreduction process is complex and involves  
69 the initial transformation of NO<sub>3</sub><sup>-</sup> into NO<sub>2</sub><sup>-</sup> ion by overall reaction (1), which is subsequently reduced  
70 to NH<sub>3</sub> according to reaction (2), via NH<sub>2</sub>OH formation, or converted into N<sub>2</sub> gas by reaction (3)  
71 through N<sub>x</sub>O<sub>y</sub> species [2,15,25]:

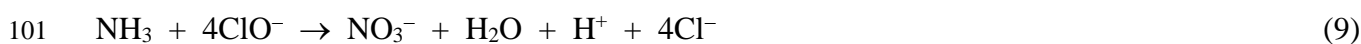
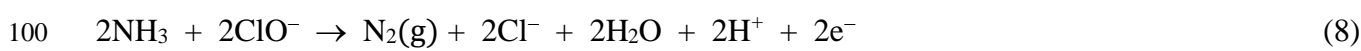


75 EO/electrodenitrification pairing using an undivided reactor appears to be an appealing  
76 alternative to increase the viability of the electrochemical technologies, since the typical parasitic  
77 oxygen evolution reaction (OER) at the anode (M) is replaced by water conversion to adsorbed  
78 hydroxyl radical (M(•OH)) via reaction (4). This is a strong oxidant that can be directly employed to  
79 degrade organic pollutants [26-28]:



81 In EO, the non-active BDD anode is more powerful than the active dimensionally stable anodes  
82 (DSA<sup>®</sup>) in chloride-free aqueous matrices because it gives large amounts of physisorbed M(•OH). In  
83 contrast, in Cl<sup>-</sup> media the oxidation power of DSA<sup>®</sup> is considerably improved due to its higher  
84 selectivity to produce active chlorine (Cl<sub>2</sub>/HClO/ClO<sup>-</sup>) via reactions (5)-(7) [28,29]. HClO with  $E^\circ =$   
85 1.36 V prevails at pH 3.0-8.0, whereas at pH > 8.0 the milder ClO<sup>-</sup> with  $E^\circ = 0.89$  V predominates.  
86 Once generated, active chlorine can oxidize NH<sub>3</sub> to N<sub>2</sub> from reaction (8) [16,30-33] or to NO<sub>3</sub><sup>-</sup> ion  
87 from reaction (9) [30,31]. Oxidation of NO<sub>2</sub><sup>-</sup> to NO<sub>3</sub><sup>-</sup> ion via reaction (10) is feasible [34], thereby  
88 reducing the global effectiveness of NO<sub>3</sub><sup>-</sup> electroreduction. Active chlorine can be anodically

89 oxidized to yield toxic and undesired  $\text{ClO}_3^-$  and  $\text{ClO}_4^-$  ions [14-16], and the process can be further  
 90 complicated by the formation of chloramines, initiated by reaction (11) [16,35,36]. Chloramines are  
 91 preferentially formed in acidic medium and can easily evolve to  $\text{N}_2$  or  $\text{N}_2\text{O}$ . Reactions (6)-(11) are  
 92 homogeneous, thus taking place in the solution bulk. Note that reactions (2), (8), (9) and (11) can  
 93 involve either  $\text{NH}_3$  in alkaline medium or its less reactive protonated form  $\text{NH}_4^+$  ( $\text{p}K_a=9.25$ ) in acidic  
 94 and circumneutral media. In the three latter reactions,  $\text{NH}_3/\text{NH}_4^+$  reacts with active chlorine in the  
 95 form of  $\text{ClO}^-/\text{HClO}$ , having the higher or lower redox potential of these oxidants a certain influence  
 96 on the conversion percentage.



104 Some authors evaluated the influence of the anode material on the  $\text{NO}_3^-$  electroreduction,  
 105 showing that in the presence of  $\text{Cl}^-$ , BDD becomes more efficient than  $\text{IrO}_2$ -based DSA<sup>®</sup> [14,16].  
 106 This unexpected behavior has been ascribed to the lower adsorption of the products, arising from  
 107 cathodic  $\text{NO}_3^-$  reduction, on BDD surface, which drastically diminishes their eventual re-oxidation.  
 108 Much less is known about the electrodenitrification process in groundwater, although a smaller  
 109 efficiency could be expected due to different detrimental factors such as the presence of natural  
 110 organic matter (NOM), the low  $\text{NO}_3^-$  concentration and the high hardness that can cause the cathode  
 111 deactivation, thus blocking the electrocatalytic reduction process [25].

112 In recent years, our group has shown the excellent oxidation power of EO and other  
113 electrochemical advanced oxidation processes to destroy pesticides in synthetic solutions [37-42] and  
114 even in groundwater [14,29]. A preliminary study about the treatment of the insecticide imidacloprid  
115 in groundwater evidenced a better performance of EO/electrodenitrification using Fe as cathode to  
116 simultaneously remove the pesticide and  $\text{NO}_3^-$  ion [14]. However, more research efforts are required  
117 to demonstrate the potential viability of paired electrolysis for groundwater remediation in view of  
118 the scarce information available so far.

119 Terbutylazine (TBZE, CAS number 5915-41-3,  $\text{C}_9\text{H}_{16}\text{ClN}_5$ , *N-tert-butyl-6-chloro-N'-ethyl-*  
120 *[1,3,5]triazine-2,4-diamine*,  $M = 229.71 \text{ g mol}^{-1}$ ) belongs to the s-triazine family, and it is one of the  
121 most used herbicides in Portugal, Italy and Spain [43]. It is a pollutant of emerging concern because  
122 its low solubility in water (about  $9 \text{ mg dm}^{-3}$  at  $20^\circ\text{C}$ ) and high affinity to soil confer large persistence  
123 in surface water, groundwater and marine water, where it has reached  $0.2 \mu\text{g L}^{-1}$ ,  $> 5 \mu\text{g L}^{-1}$  and  $84$   
124  $\text{ng L}^{-1}$  in EU countries, respectively. Note that  $0.1 \mu\text{g L}^{-1}$  is the recommended maximum content in  
125 drinking water, according to EU Directives [43,44]. TBZE is very toxic to living beings at low doses  
126 due to its ability to bioaccumulate, posing high long-term risks to non-target plants and soil  
127 macroinvertebrates, mammals and aquatic organisms [43]. It is decomposed to desethylterbutylazine  
128 (DE-TBZE), which is also largely persistent in water and even more toxic than the parent herbicide  
129 [44]. Several works have reported a large removal of TBZE from water by simple separation methods  
130 involving adsorption on membranes [45], selective polymeric materials [46], activated carbon and  
131 carbon nanotubes [47] and metal-organic frameworks [48]. Transformation techniques including  
132  $\text{O}_3$ /activated carbon, solar/ $\text{O}_3$  and solar/ $\text{TiO}_2/\text{O}_3$  [47], UV/ $\text{H}_2\text{O}_2$  [47,49], UV/ $\text{TiO}_2$ /chitosan [50] and  
133 UV/B-doped  $\text{TiO}_2/\text{O}_3$  [51] have been tested as well. Tasca et al. [52] used a zero-gap cell equipped  
134 with a BDD mesh anode, a  $\text{RuO}_2$  mesh cathode and a solid polymer electrolyte, to degrade  $300 \text{ cm}^3$   
135 of  $4 \text{ mg dm}^{-3}$  TBZE in deionized water by EO. About 89% and 97% of pesticide removal was attained

136 after 60 min at 100 and 500 mA, respectively, with energy consumptions  $< 11 \text{ kWh m}^{-3}$ . Note that  
137 the target herbicide possesses 5 N atoms that can be released to contribute to  $\text{NO}_3^-$  accumulation.

138 To gain a better insight on the EO/electrodenitrification process, here we report the simultaneous  
139 TBZE electrochemical oxidation and  $\text{NO}_3^-$  electroreduction in actual groundwater matrix. Key  
140 experimental parameters like  $I$  and pH were systematically assessed. The experiments were carried  
141 out with an undivided tank reactor equipped with a BDD or  $\text{RuO}_2$  (i.e.,  $\text{DSA}^{\text{®}}\text{-Cl}_2$ ) anode and an Fe  
142 cathode. Prior to electrolysis with groundwater matrix, the sample was softened to minimize the  
143 content of alkaline earth metal ions, a crucial step to avoid the loss of cathode electroactivity upon  
144 precipitation of hydroxides and carbonates. Comparative assays were performed with simulated  
145 solutions mimicking the anionic composition of the softened groundwater to clarify the evolution of  
146  $\text{NO}_3^-$  and generated ions and the role of NOM. TBZE was always spiked into the aqueous matrices  
147 at a concentration as high as  $5.0 \text{ mg dm}^{-3}$  in order to minimize the quantification error of all  
148 concentrations, thus providing reliable degradation kinetics data. The total nitrogen (TN)  
149 concentration decay in solution was monitored as well. A post-treatment with an ion exchange resin  
150 was implemented as a final conditioning step to reduce the impact of the oxychlorine anions  
151 produced.

## 152 **2. Materials and methods**

### 153 *2.1. Chemicals*

154 Analytical standards (PESTANAL<sup>®</sup>) terbuthylazine and desethylterbuthylazine were purchased  
155 from Sigma. The solution pH was regulated with analytical grade  $\text{H}_2\text{SO}_4$  (95-98%) and NaOH (98-  
156 100%) purchased from Panreac. Simulated water matrices were prepared with analytical grade  
157 electrolytes, including KCl ( $> 99\%$ ) provided by Sigma-Aldrich, and  $\text{KNO}_3$  (98%) and  $\text{K}_2\text{SO}_4$   
158 (99.9%) supplied by Panreac. Other chemicals and solvents used were either of analytical or high-  
159 performance liquid chromatography (HPLC) grade provided by Aldrich, Fluka, Lancaster and

160 Panreac. Ultrapure water (Millipore Milli-Q, > 18.2 MΩ cm) was used to prepare the analytical  
161 solutions and simulated water matrices.

## 162 2.2. Aqueous matrices

163 Actual groundwater was collected from a water well located in an agricultural land in the  
164 surroundings of Barcelona (Spain). The sample was softened following three consecutive steps: (i)  
165 alkalization up to pH 11.5 by adding 1 M NaOH solution, (ii) sedimentation for 24 h and filtration  
166 with regenerated cellulose filter membrane (0.45 μm) to remove the precipitated carbonates and  
167 hydroxides and, finally, (iii) acidification with 1 M H<sub>2</sub>SO<sub>4</sub> solution to reach the desired pH. The  
168 resulting softened groundwater was preserved in a refrigerator at 4 °C before usage for electrolytic  
169 treatments. Table 1 collects the physicochemical parameters of: (i) the raw groundwater; (ii) the  
170 softened groundwater once conditioned at pH 4.0 and with TBZE spiked at a concentration of 5.0 mg  
171 dm<sup>-3</sup>; (iii) that softened groundwater, after an electrochemical treatment for 360 min; and (iv) the  
172 solution resulting from such electrolysis, after treatment with a Purolite® A532E resin, a polystyrenic  
173 strong base anion gel in the chloride form that is recommended by the provider for perchlorate  
174 removal. As can be seen, the softening process led to a drastic reduction of the concentration of all  
175 alkaline earth metal ions, whereas the Na<sup>+</sup> and SO<sub>4</sub><sup>2-</sup> concentrations substantially grew up. This  
176 sample showed low conductivity and total organic carbon (TOC), whereas its TN content mainly  
177 corresponded to NO<sub>3</sub><sup>-</sup>. The final post-treatment with the resin allowed the reduction of the ClO<sub>3</sub><sup>-</sup>,  
178 NO<sub>3</sub><sup>-</sup> and SO<sub>4</sub><sup>2-</sup> concentrations alongside the complete removal of ClO<sub>4</sub><sup>-</sup>, with a concomitant increase  
179 in the Cl<sup>-</sup> content.

180 Three simulated water samples were prepared to separately assess the behavior of the main  
181 anions contained in the softened groundwater. The conductivity of such solutions at neutral pH was  
182 around 1.7-1.8 mS cm<sup>-1</sup> and their composition was: (i) 10 mM K<sub>2</sub>SO<sub>4</sub> (980 mg dm<sup>-3</sup> SO<sub>4</sub><sup>2-</sup>); (ii) 1.6  
183 mM KNO<sub>3</sub> (100 mg dm<sup>-3</sup> NO<sub>3</sub><sup>-</sup>) + 7.6 mM K<sub>2</sub>SO<sub>4</sub> (745 mg dm<sup>-3</sup> SO<sub>4</sub><sup>2-</sup>); and (iii) 10 mM KCl (355  
184 mg dm<sup>-3</sup> Cl<sup>-</sup>) + 1.6 mM KNO<sub>3</sub> (100 mg dm<sup>-3</sup> NO<sub>3</sub><sup>-</sup>) + 0.8 mM K<sub>2</sub>SO<sub>4</sub> (78 mg dm<sup>-3</sup> SO<sub>4</sub><sup>2-</sup>). The pH of



185 these solutions was adjusted to 4.0, 7.0 and 10.5 and they were electrolyzed, in the absence or  
186 presence of  $5.0 \text{ mg dm}^{-3}$  TBZE, without pH regulation.

### 187 *2.3. Electrolytic system*

188 The electrolytic assays were performed in an undivided glass tank reactor, which had a jacket to  
189 continuously recirculate thermostated water at 25 °C. Each experiment was made with  $500 \text{ cm}^3$  of  
190 solution, which was kept under stirring with a magnetic follower at 900 rpm. The anode was either a  
191 Nb mesh coated with a  $5 \text{ }\mu\text{m}$  BDD thin film (3,500 ppm B), purchased from Condias, or a  $\text{RuO}_2$  mesh  
192 purchased from De Nora, whereas a custom iron mesh (Fe, 99.9%) was used as the cathode. The  
193 surface of the anode and cathode immersed into the solution had dimensions of  $3.5 \text{ cm} \times 7.5 \text{ cm}$ . The  
194 electrodes were placed in the center of the tank reactor, separated at a distance of 3 mm. In some  
195 cases, two Fe cathodes were used, with the anode sandwiched between them keeping a separation of  
196 3 mm with each cathode. The electrolyses were carried out under galvanostatic conditions with an  
197 Amel 2051 potentiostat-galvanostat providing a constant current ( $I$ ) of 250, 500 or 1000 mA. A  
198 Demestres 601BR digital multimeter was used to monitor the potential difference between the  
199 electrodes. Before each experiment, the Fe cathode was consecutively polished with P240 and P800  
200 sandpapers, submerged in a 20%  $\text{H}_2\text{SO}_4$  solution, rinsed with Milli-Q water and dried at room  
201 temperature.

### 202 *2.4. Analytical procedures*

203 A Metrohm 644 conductometer and a Crison 2200 pH-meter were used to determine the solution  
204 conductance and pH, respectively. A periodic withdrawal of  $1.5 \text{ cm}^3$  of treated samples from the tank  
205 reactor was made for analysis, followed by filtration with Whatman  $0.45 \text{ }\mu\text{m}$  PTFE membrane filters.

206 TN measurements were made with a Shimadzu VCSN TOC analyzer coupled to a TNM-1 unit.  
207 The nitrogen mass balance at the end of each assay was made considering the  $\text{NO}_2^-$ ,  $\text{NO}_3^-$  and  $\text{NH}_4^+$   
208 concentrations detected, the solution TN value at each time to account for other soluble N-species  
209 and the initial TN of the sample to ascertain the quantity of volatiles released. Free chlorine and total

210 chlorine contents were obtained by the *N,N*-diethyl-*p*-phenylenediamine colorimetric method, using  
211 an Unicam UV4 UV/Vis spectrophotometer at  $\lambda = 515$  nm [53]. The concentration of  $\text{Cl}^-$ ,  $\text{ClO}_3^-$ ,  
212  $\text{ClO}_4^-$ ,  $\text{NO}_2^-$ ,  $\text{NO}_3^-$  and  $\text{NH}_4^+$  ions was obtained following the procedures described elsewhere [54].  
213 The content of iron, calcium, magnesium ions and the other elements in solution was determined by  
214 inductively coupled plasma with optical emission spectroscopy (ICP-OES) on a Perkin Elmer Optima  
215 8300 spectrometer.

216 The TBZE concentration was monitored by reversed-phase HPLC using a Waters 600 liquid  
217 chromatograph (LC) coupled to a 996 photodiode array detector. Aliquots of 20  $\mu\text{L}$  were injected into  
218 the LC and the separation of organics was achieved by means of a Spherisorb® S5 ODS2 5  $\mu\text{m}$  (150  
219  $\text{mm} \times 4.6$  mm (i.d.)) column at 35 °C, upon elution with a 60:40 (v/v) acetonitrile/water mixture at  
220  $1.0 \text{ cm}^3 \text{ min}^{-1}$ . Using Empower® software for control, the peak for TBZE ( $\lambda = 222.9$  nm) appeared at  
221 retention time ( $t_r$ ) of 7.8 min, with L.O.Q =  $0.32 \text{ mg dm}^{-3}$  and L.O.D =  $0.11 \text{ mg dm}^{-3}$ . The peak for  
222 DE-TBZE ( $\lambda = 214.7$  nm) appeared at  $t_r = 4.1$  min, with L.O.Q =  $0.59 \text{ mg dm}^{-3}$  and L.O.D =  $0.19 \text{ mg}$   
223  $\text{dm}^{-3}$ .

224 The same LC was equipped with a Bio-Rad Aminex HPX 87H (300 mm  $\times$  7.8 mm (i.d.)) column  
225 at 35 °C, its detector selected at  $\lambda = 210$  and a 4 mM  $\text{H}_2\text{SO}_4$  solution flowing at  $0.6 \text{ cm}^3 \text{ min}^{-1}$  as  
226 mobile phase, to quantify the produced acids by ion-exclusion HPLC. The acids detected were oxalic  
227 ( $t_r = 7.3$  min), oxamic ( $t_r = 10.3$  min) and cyanuric ( $t_r = 12.6$  min).

228 The experiments were always made in duplicate, and average results are reported. Figures show  
229 the corresponding error bars within a 95% confidence interval.

230 Solutions of  $5.0 \text{ mg dm}^{-3}$  TBZE spiked into a simulated water matrix at pH 4.0 and 25 °C were  
231 electrolyzed for 60 min using a BDD/Fe cell at  $I = 500$  mA. The organics were extracted with  $\text{CH}_2\text{Cl}_2$   
232 ( $3 \times 50 \text{ cm}^3$ ). The organic phase was then dried over anhydrous  $\text{Na}_2\text{SO}_4$ , filtered and its volume  
233 reduced to ca.  $2 \text{ cm}^3$  under  $\text{N}_2$  stream for analysis by gas chromatography-mass spectrometry (GC-  
234 MS). The analysis was performed by equipping the gas chromatograph with either a polar Agilent

235 HP-INNOWax GC or a non-polar Teknokroma Sapiens X5-MS column, following the same  
236 procedures detailed in earlier work [55]. The mass spectra of heteroaromatic products formed from  
237 the initial TBZE degradation were compared with those found in the NIST05 database.

### 238 **3. Results and discussion**

#### 239 *3.1. Electrodennitrication of simulated groundwater without herbicide*

240 A first series of experiments was performed to clarify the effect of pH on the  $\text{NO}_3^-$   
241 electroreduction, in the absence of pesticide. This was made by electrolyzing 500 cm<sup>3</sup> of solutions  
242 with 100 mg dm<sup>-3</sup>  $\text{NO}_3^-$  + 7.6 mM  $\text{SO}_4^{2-}$  at initial pH of 4.0, 7.0 and 10.5 using BDD/Fe and  $\text{RuO}_2/\text{Fe}$   
243 tank reactors at  $I = 500$  mA. Table 2 shows that the acidic and neutral solutions were strongly  
244 alkalinized, attaining final pH values of 10.3-10.8 and 10.1-11.2 in the cells with BDD and  $\text{RuO}_2$ ,  
245 respectively, as expected from the  $\text{OH}^-$  generation upon consecutive reduction of  $\text{NO}_3^-$  to  $\text{NO}_2^-$ ,  $\text{NH}_3$   
246 and  $\text{N}_2$  via reactions (1)-(3) [14]. The high  $\text{OH}^-$  content at initial pH 10.5 can explain the small pH  
247 variation ( $\pm 0.5$  units) found in that medium regardless of the anode used (see Table 2).

248 Fig. 1a presents the variation of  $\text{NO}_3^-$  concentration with electrolysis time. Using BDD anode,  
249 similar decays can be observed at all pH values, with a reduction of 75%-78% at the end of the  
250 treatment. This good result can be related to the poor adsorption of the products originated from  $\text{NO}_3^-$   
251 electroreduction (e.g.,  $\text{NH}_4^+$  ion) on the BDD surface regardless of the pH. As a result, their  
252 subsequent re-oxidation to the parent anion occurred only to a small extent, which was positive in  
253 terms of global nitrate removal [15,16]. In contrast, a fluctuating behavior occurred in the cell with  
254  $\text{RuO}_2$  anode, with up to 87% of  $\text{NO}_3^-$  removal at pH 4.0, 81% at pH 10.5 but only up to 56% at pH  
255 7.0. This means that at the latter pH, the products of  $\text{NO}_3^-$  electroreduction are more largely adsorbed  
256 onto the  $\text{RuO}_2$  surface, favoring their faster re-oxidation. According to these findings, the use of BDD  
257 is more favorable for electrodenitrication at neutral pH, whereas  $\text{RuO}_2$  becomes slightly superior in  
258 acidic and alkaline media. Fig. 1b depicts that the above concentration decays obeyed a pseudo-first-

259 order kinetics, and the apparent rate constants ( $k(\text{NO}_3^-)$ ) are collected in Table 2. As expected from  
260 the trends of Fig. 1, similar  $k(\text{NO}_3^-)$  values between  $4.6 \times 10^{-3}$  and  $5.2 \times 10^{-3} \text{ min}^{-1}$  were obtained in  
261 the trials with BDD, which rose up to  $6.3 \times 10^{-3} \text{ min}^{-1}$  for the faster abatement at pH 4.0 using  $\text{RuO}_2$ .

262 The accumulated  $\text{NH}_4^+$  content increased gradually as the  $\text{NO}_3^-$  concentration disappeared, as  
263 can be seen in Fig. 1c. About  $20 \text{ mg dm}^{-3}$  as maximal and  $12 \text{ mg dm}^{-3}$  as minimal of  $\text{NH}_4^+$  were finally  
264 obtained. A certain TN abatement was found in all the assays, varying between 9.0% and 18%, which  
265 can be related to the loss of volatile N-compounds (see Fig. 1d). The speciation of N-containing  
266 compounds at the end of all electrolyses shown in Fig. 1e reveals the preeminence of  $\text{NH}_4^+$  ion over  
267 all the other species, suggesting the leading role of consecutive reactions (1) and (2) in the  
268 electrodenitrification process with Fe cathode. The production of volatile N-compounds, like  $\text{N}_x\text{O}_y$   
269 and  $\text{N}_2$  via reaction (3) is then a less favorable reduction route. Note that at the final alkaline pH  
270 values achieved, the acid/base equilibrium of  $\text{NH}_4^+$  ion ( $\text{p}K_a = 4.75$ ) results in the accumulation of its  
271 conjugated form, which can contribute to the N-volatiles.

272 Data of Table 2 also show higher average cell potentials ( $E_{\text{cell}}$ ) using BDD, owing to the higher  
273 potential required for water discharge as compared to that needed with  $\text{RuO}_2$  [26]. The energy  
274 consumption (EC) of the process, calculated as  $\text{EC} = E_{\text{cell}} I t / V$ , was then greater for BDD (45.0-50.4  
275  $\text{kWh m}^{-3}$  vs 39.0-41.2  $\text{kWh m}^{-3}$ ).

276 The above study was extended to a  $10 \text{ mM Cl}^- + 100 \text{ mg dm}^{-3} \text{ NO}_3^- + 0.8 \text{ mM SO}_4^{2-}$  solution to  
277 explore the effect of  $\text{Cl}^-$  oxidation on the  $\text{NO}_3^-$  electroreduction. These trials were carried out starting  
278 at pH 4.0, 7.0 and 10.5 using both cells at  $I = 500 \text{ mA}$ . In addition, with the BDD anode, the effect of  
279  $I$  was studied at pH 4.0. After 360 min, Table 2 shows that final pH values with BDD were similar to  
280 those mentioned for chloride-free solutions, whereas they tended to be slightly lower (8.4-10.0) using  
281  $\text{RuO}_2$ . This behavior suggests that the greater production of active chlorine with the latter anode  
282 resulted in a relevant contribution of reactions (9)-(10), eventually leading to a smaller global  
283 electrodenitrification with lower  $\text{OH}^-$  net production from reactions (1)-(3). This hypothesis is

284 confirmed from the profiles of Fig. 2a, where the  $\text{NO}_3^-$  concentration decays more slowly using  $\text{RuO}_2$ .  
285 The  $\text{NO}_3^-$  content was progressively reduced by 79%, 76% and 65% at pH 4.0, 7.0 and 10.5 using  
286 BDD, becoming slower until reaching 62%, 60% and 47% removal with  $\text{RuO}_2$ . Good linear  
287 correlations related to a pseudo-first order process were found for all these trends (see Fig. 2b), giving  
288 rise to lower  $k(\text{NO}_3^-)$  values as compared to those determined in the absence of chloride (see Table  
289 2). The loss of efficiency of  $\text{NO}_3^-$  electroreduction in the chloride medium can be accounted for by  
290 the anodic generation of active chlorine ( $\text{HClO}$  and/or  $\text{ClO}^-$ ) via reactions (5)-(7), which then reacts  
291 with  $\text{NH}_4^+$  (largely formed from  $\text{NO}_3^-$  reduction, as shown in Fig. 1c) to originate  $\text{N}_2$  gas via reaction  
292 (8), regenerate  $\text{NO}_3^-$  ion via reactions (9) and (10) or produce chloramines via reaction (11). The  
293 oxidation of electroreduction products by active chlorine contributed to slow down the global  
294 electrodenitrification. Moreover, the progressive deceleration of  $\text{NO}_3^-$  electroreduction with decrease  
295 of  $k(\text{NO}_3^-)$  was much more remarkable when changing the starting pH from neutral to alkaline (see  
296 Fig. 2a and Table 2). This phenomenon can be ascribed to the conversion of  $\text{HClO}$  to  $\text{ClO}^-$ , which  
297 behaves as a more reactive species, either promoting the oxidation of N-species to  $\text{NO}_3^-$  or competing  
298 with  $\text{NO}_3^-$  electroreduction. On the other hand, Fig. 2a also shows a more effective  
299 electrodenitrification when  $I$  was increased from 250 to 1000 mA at pH 4.0 using BDD, with the  
300 highest  $\text{NO}_3^-$  removal of 82% attained upon application of the greatest  $I$ . The corresponding  $k(\text{NO}_3^-)$   
301 values of Table 2 were upgraded from  $3.3 \times 10^{-3}$  to  $6.1 \times 10^{-3} \text{ min}^{-1}$  (1.85-fold) upon a 4-fold rise of  
302  $I$  from 250 to 1000 mA, pointing to a larger influence of  $\text{NH}_4^+$  re-oxidation at higher  $I$ .

303 The effect of reactions (8)-(11) on electrodenitrification was confirmed by analyzing the  
304 evolution of generated  $\text{NH}_4^+$  and TN. No  $\text{NH}_4^+$  was detected using the  $\text{RuO}_2$  anode. Fig. 2c shows  
305 that the amount of this ion accumulated in the medium using the BDD anode depended on the applied  
306  $I$ . While  $\text{NH}_4^+$  was not found at 250 mA, it was accumulated between 2.2 and 2.9  $\text{mg dm}^{-3}$  at 500 mA  
307 and much more largely (up to 10.0  $\text{mg dm}^{-3}$ ) at 1000 mA, in agreement with the faster  $\text{NO}_3^-$

308 electroreduction. Much larger TN removals were attained in the chloride medium (see Fig. 2d) as  
309 compared to those in the chloride-free one (see Fig. 1d), which is explained by the loss of much  
310 greater amounts of volatile N-compounds, mainly N<sub>2</sub>. For example, up to 65.5% of volatiles was  
311 released as maximal at initial pH 7.0 with a BDD anode at 500 mA, much superior to 12.5% found  
312 in the absence of chloride. Active chlorine reacts with the generated NH<sub>4</sub><sup>+</sup> via reaction (8), reaching  
313 the breakpoint chlorination at a pH at which the HClO and NH<sub>4</sub><sup>+</sup> species have the maximum  
314 reactivity, enhancing the production of volatile N-compounds especially at an initial pH of 7.0. At  
315 initial pH 10.5, the acid/base equilibrium of NH<sub>4</sub><sup>+</sup> ion (pK<sub>a</sub> =9.25) is shifted toward NH<sub>3</sub>, the most  
316 reactive form with active chlorine, but ClO<sup>-</sup> has a lower oxidation power than its acidic counterpart,  
317 yielding a lower amount of volatile N-compounds. From these results, the speciation of the final N-  
318 compounds is depicted in Fig. 2e. As can be seen, the residual NO<sub>3</sub><sup>-</sup> and, more significantly, the  
319 volatile N-compounds in most cases were the predominant species. This means that the reduction of  
320 NO<sub>3</sub><sup>-</sup> to NH<sub>4</sub><sup>+</sup> via reaction (2), followed by the conversion of NH<sub>4</sub><sup>+</sup> to N<sub>2</sub> via reaction (8), are the  
321 preferential electrodenitrification steps occurring in the chloride matrix.

322 Fig. 3a shows the decay of Cl<sup>-</sup> concentration for the runs performed in the chloride media. Two  
323 trends can be observed: (i) a slow abatement of the ion using RuO<sub>2</sub>, achieving close to 47% removal  
324 regardless of the pH; and (ii) a faster removal with BDD that was highly dependent on the applied *I*,  
325 yielding increasing final removals of 75%, 93% and 96% at 250, 500 and 1000 mA, respectively, at  
326 pH 4.0. This agrees with the tendencies of the *k*(Cl<sup>-</sup>) values listed in Table 2 for such assays, obtained  
327 from the excellent linear profiles shown in Fig. 3b assuming a pseudo-first-order reaction. The slow  
328 Cl<sup>-</sup> removal found using RuO<sub>2</sub> is indicative of its main electrodic oxidation via reaction (5). In  
329 contrast, its quicker destruction using BDD can be ascribed to the action not only of reaction (5), but  
330 also to its reaction with BDD(•OH) originated from reaction (4), which is a more powerful oxidant  
331 than RuO<sub>2</sub>(•OH). It is noticeable that for BDD, the rise of *k*(Cl<sup>-</sup>) value showed good proportionality  
332 with *I*, changing from 3.4 × 10<sup>-3</sup> min<sup>-1</sup> at 250 mA to 1.24 × 10<sup>-2</sup> min<sup>-1</sup> at 1000 mA (see Table 2). This

333 suggests an almost linear enhancement of the rate of reactions (4) and (5) to destroy the ion. It is well  
334 known that further conversion of  $\text{Cl}^-$  into active chlorine is complicated with BDD due to the  
335 subsequent generation of  $\text{ClO}_3^-$  and  $\text{ClO}_4^-$  ions as follows [26]:



339 The time course of both ions for the same trials is presented in Fig. 3c and 3d. As can be seen,  
340 when a  $\text{RuO}_2$  anode was used, low  $\text{ClO}_3^-$  contents up to  $120 \text{ mg dm}^{-3}$  were always determined at all  
341 pH values, whereas no  $\text{ClO}_4^-$  was found. This behavior indicates that this anode allowed reactions  
342 (12) and (13) to some extent, but reaction (14) was completely inhibited. In contrast, much higher  
343  $\text{ClO}_3^-$  concentrations were found with BDD, thanks to the parallel reaction with  $\text{BDD}(\bullet\text{OH})$ . In fact,  
344 Fig. 3c shows a similar  $\text{ClO}_3^-$  evolution at all pH values and a decay of its accumulated content with  
345 raising  $I$  due to its fast reaction with  $\text{BDD}(\bullet\text{OH})$  to obtain much greater amounts of  $\text{ClO}_4^-$  as the  
346 electrolysis was prolonging (see Fig. 3d). For example, at the highest  $I$  of 1000 mA, a  $\text{ClO}_4^-$   
347 concentration as high as  $925 \text{ mg dm}^{-3}$  was determined, being much higher than  $35 \text{ mg dm}^{-3}$  obtained  
348 for  $\text{ClO}_3^-$  ion. These two ions were the main oxidation products of  $\text{Cl}^-$  with BDD, since no active  
349 chlorine was detected at the end of most treatments.

350 The similar conductivity of media prepared with and without chloride allowed obtaining an  
351 analogous  $E_{\text{cell}}$  at a given  $I$ , giving rise to EC values similar to those mentioned above (see Table 2).  
352 As expected,  $E_{\text{cell}}$  and EC increased dramatically with increasing  $I$ , attaining excessively high values  
353 of 13.5 V and  $162.0 \text{ kWh m}^{-3}$  at 1000 mA, although the higher electrodenitrification power could  
354 justify the operation at such high input current.

### 355 3.2. Electrochemical oxidation of terbuthylazine in sulfate medium

356 The oxidation ability of the BDD/Fe cell to remove TBZE from 500 cm<sup>3</sup> of a 10 mM Na<sub>2</sub>SO<sub>4</sub>  
357 solution with 5.0 mg dm<sup>-3</sup> herbicide at pH 4.0 by EO was assessed at 500 mA for 360 min. The  
358 solution pH slightly increased, whereas the  $E_{\text{cell}}$  of 8.3 V was analogous to the above matrices with  
359 similar conductivity, resulting in an EC close to 50 kWh m<sup>-3</sup> (see Table 2).

360 Fig. 4a highlights the fast herbicide abatement with electrolysis time, completely disappearing  
361 from the medium in 80 min. Its concentration followed a pseudo-first-order decay, as depicted in the  
362 inset of Fig. 4a, with an apparent rate constant  $k(\text{TBZE}) = 9.0 \times 10^{-2} \text{ min}^{-1}$ , much greater than that  
363 found for Cl<sup>-</sup> oxidation (see Fig. 3a and Table 2). This is indicative of a quick reaction of the target  
364 herbicide with a constant concentration of BDD(<sup>•</sup>OH) formed from reaction (4).

365 The intermediates and final products formed during the EO process were analyzed as well. The  
366 reversed-phase HPLC chromatograms revealed the production of DE-TBZE as main heteroaromatic  
367 byproduct. It was rapidly accumulated up to 0.59 mg dm<sup>-3</sup> at 10 min, further being completely  
368 removed in 150 min (see Fig. 4b). Fig. 4c shows that the NH<sub>4</sub><sup>+</sup> concentration grew continuously up  
369 to 0.73 mg N dm<sup>-3</sup>, while NO<sub>3</sub><sup>-</sup> was accumulated up to 0.69 mg N dm<sup>-3</sup>, accounting for a 47.8% and  
370 45.3% of the 1.525 mg N dm<sup>-3</sup> contained in the herbicide, respectively. This suggests the presence of  
371 other more recalcitrant N-products in the final solution, considering the low ability of BDD to produce  
372 N<sub>2</sub> (see Fig. 1e). Oxalic, oxamic and cyanuric acids were identified by ion-exclusion HPLC. The two  
373 former carboxylic acids are final byproducts that are directly transformed into CO<sub>2</sub>, whereas cyanuric  
374 acid is the most stable byproduct in the degradation of s-triazines [56]. As can be seen in Fig. 4d, only  
375 oxalic acid was completely removed in 120 min, whereas the other acids were very persistent, thereby  
376 impeding the overall mineralization of TBZE.

### 377 3.3. Electrochemical oxidation/electrodenitrification process in simulated groundwater

378 The paired EO/electrodenitrification using the BDD/Fe and RuO<sub>2</sub>/Fe tank reactors was studied  
379 with a 5.0 mg dm<sup>-3</sup> TBZE + 100 mg dm<sup>-3</sup> NO<sub>3</sub><sup>-</sup> + 7.6 mM SO<sub>4</sub><sup>2-</sup> solution at pH 4.0 and 500 mA. As  
380 in the cases discussed above, the solution pH raised up to ca. 10 after 360 min of electrolysis, the  $E_{\text{cell}}$



381 value was slightly superior with the BDD anode, and EC values were similar to those found without  
382 the herbicide (see Table 2). Fig. 5a highlights a much faster TBZE removal using BDD. The herbicide  
383 was completely abated in 120 min, a time higher than 80 min needed in sulfate medium (see Fig. 4a),  
384 suggesting that the anodic oxidation of  $\text{NH}_4^+$  diminishes the amount of BDD( $\bullet\text{OH}$ ) available for  
385 TBZE destruction. In contrast, the herbicide concentration was reduced by 89% using  $\text{RuO}_2$ , in  
386 agreement with the much smaller oxidation power of  $\text{RuO}_2(\bullet\text{OH})$ . This behavior can be confirmed  
387 from the corresponding  $k(\text{TBZE})$  values, which were 9.0-fold higher using BDD (see Table 2). The  
388 intermediate DE-TBZE was not detected with this anode, in contrast to that found in sulfate medium  
389 (see Fig. 4b), probably because it was accumulated to a smaller amount during the whole electrolysis.  
390 This phenomenon did not occur with  $\text{RuO}_2$  due to its lower oxidation ability, and DE-TBZE was  
391 largely accumulated without apparent destruction, attaining a steady value  $1.49 \text{ mg dm}^{-3}$  as can be  
392 seen in Fig. 5b. The aforementioned behavior can be confirmed from the  $\text{NO}_3^-$  abatements shown in  
393 Fig. 5c. Using the  $\text{RuO}_2$  anode, the content decayed with a  $k(\text{NO}_3^-)$  value of  $6.5 \times 10^{-3} \text{ min}^{-1}$ . This is  
394 similar to that determined in the absence of the herbicide (see Table 2), denoting that EO and  
395 electroreduction behave as independent processes using  $\text{RuO}_2$ . In contrast, the interaction of both  
396 processes using BDD caused 0.5-fold drop of  $k(\text{NO}_3^-)$  in the presence of the herbicide, pointing to  
397 the  $\text{NO}_3^-$  generation during the pesticide degradation. This was confirmed by the fact that in the final  
398 solution treated with BDD, small contents of  $\text{NO}_2^-$  ion were detected alongside a much smaller  $\text{NH}_4^+$   
399 accumulation (see Fig. 5d). As in the case of the chloride-free medium without the herbicide, in the  
400 presence of this latter pollutant a very low TN removal could be observed (Fig. 5e). Hence,  $\text{NO}_3^-$   
401 evolved mainly to  $\text{NH}_4^+$  via reaction (2) and, to a much smaller extent, to  $\text{N}_2$  gas via reaction (3). The  
402 speciation of the final N-compounds depicted in Fig. 5f confirms this behavior, showing that the  
403 generated  $\text{NH}_4^+$  ion and the residual  $\text{NO}_3^-$  ion were the main N-species regardless of the anode. Note  
404 that the N initially contained in the herbicide was not measured with the TN analyzer, but this N (10%  
405 of the total TN) appeared gradually as the herbicide byproducts were formed, which justifies the

406 normalized TN values greater than 1.0 in Fig. 5e. This was more significant using BDD due to its  
407 greater power to destroy TBZE.

408 The study was completed with the case of a simulated matrix with chloride (10 mM  $\text{Cl}^-$  + 100  
409  $\text{mg dm}^{-3} \text{NO}_3^-$  + 0.8 mM  $\text{SO}_4^{2-}$ ). TBZE was spiked at a concentration of 5.0  $\text{mg dm}^{-3}$ , and the effect  
410 of initial pH from 4.0 to 10.5 and applied  $I$  from 250 to 1000 mA was evaluated with both cells.  
411 Comparison of the data of Table 2 for these assays allows concluding that analogous final pH,  $E_{\text{cell}}$   
412 and EC values were obtained in the absence and presence of TBZE. As expected, the latter two  
413 parameters underwent a progressive rise at higher  $I$ , with the consequent acceleration of all electrodic  
414 reactions.

415 For the cell with the BDD anode, Fig. 6a shows a gradual deceleration of the herbicide  
416 disappearance as the pH was risen from 4.0 to 10.5 at each given  $I$ , with a concomitant longer time  
417 needed for total removal. This tendency can also be deduced from the corresponding  $k(\text{TBZE})$  values  
418 collected in Table 2. For example, at 500 mA, the herbicide disappeared after 50, 60 and 100 min at  
419 pH 4.0, 7.0 and 10.5, related to decreasing  $k(\text{TBZE})$  values of  $9.9 \times 10^{-2}$ ,  $5.7 \times 10^{-2}$  and  $5.2 \times 10^{-2}$   
420  $\text{min}^{-1}$ . Note that at the best pH of 4.0, a slightly quicker herbicide destruction was attained in the  
421 presence of chloride, as compared to sulfate medium ( $k(\text{TBZE}) = 9.0 \times 10^{-2} \text{min}^{-1}$ ) and chloride-free  
422 matrix ( $k(\text{TBZE}) = 5.7 \times 10^{-2} \text{min}^{-1}$ ). This can be explained by its simultaneous reaction with  
423 BDD( $\cdot\text{OH}$ ) formed via reaction (4) and active chlorine ( $\text{HClO}$ ) generated via reactions (5) and (6),  
424 which accelerated its destruction. The change of this active chlorine form to the weaker oxidant  $\text{ClO}^-$   
425 can justify the loss of oxidation power when starting at pH 7.0 and 10.5. Fig. 6a also shows that, at  
426 each pH, TBZE decayed more rapidly at higher  $I$ , as result of the greater production of BDD( $\cdot\text{OH}$ )  
427 and active chlorine.

428 The rate of  $\text{NO}_3^-$  concentration decay in the chloride medium was slightly lower with the  
429 herbicide (see Fig. 6b) than in its absence (see Fig. 2a). This trend can also be established from the  
430 lower  $k(\text{NO}_3^-)$  values determined in the former case, listed in Table 2. In the presence of TBZE, part

431 of the active chlorine oxidizes the organics, yielding additional amounts of  $\text{NO}_3^-$  ion. This was  
432 confirmed by the very low  $\text{NH}_4^+$  concentration measured at pH 4.0, which was higher at pH 7.0 and  
433 10.5. Large decays of TN were obtained in the chloride medium with herbicide, as shown in Fig. 6c,  
434 in agreement with the discussion in the absence of organics (subsection 3.1). The process was slightly  
435 slower at pH 10.5, although large amounts of volatile products ( $\text{N}_2$ ) were always formed. The analysis  
436 of the distribution of final N-species shown in Fig. 6d makes in evidence that up to 57% of volatile  
437 products were produced, corroborating that reaction (8) becomes the most important step for  $\text{NO}_3^-$   
438 removal in the presence of  $\text{Cl}^-$ . However, a smaller proportion of volatile compounds was detected  
439 as compared to the chloride matrix without herbicide (see Fig. 2d), owing to the partial loss of active  
440 chlorine resulting from its participation in the degradation of the organic molecules.

441 Fig. 6e reveals that generated active chlorine was rapidly accumulated up to around  $90 \text{ mg dm}^{-3}$   
442 as maximal, being subsequently destroyed in all cases after 360 min of electrolysis. Only at pH 10.5  
443 some small amounts persisted working at 250 and 500 mA. Although active chlorine attacks the  
444 organics and  $\text{NH}_3$ , with BDD it is mainly destroyed through direct and/or BDD( $\bullet\text{OH}$ )-mediated  
445 oxidation to  $\text{ClO}_3^-$  and  $\text{ClO}_4^-$  ions. Fig. 6f shows the rapid formation of  $\text{ClO}_3^-$  ion, which was more  
446 rapidly destroyed at increasing  $I$  to yield a large amount of the stable  $\text{ClO}_4^-$  ion (see Fig. 6g). Fig. 6f  
447 and 6g highlight that the evolution of both ions only depended on  $I$ , being quite similar to that  
448 determined without organics (see Fig. 3c and 3d).

449 The results obtained for the EO/electrodenitrification of a solution containing  $5.0 \text{ mg dm}^{-3}$  TBZE  
450 in  $10 \text{ mM Cl}^- + 100 \text{ mg dm}^{-3} \text{NO}_3^- + 0.8 \text{ mM SO}_4^{2-}$  using the  $\text{RuO}_2/\text{Fe}$  tank reactor are presented in  
451 Fig.7a-7f. Similar trends to those described for the BDD/Fe cell can be observed, but with notable  
452 differences that can be ascribed to the smaller ability of  $\text{RuO}_2(\bullet\text{OH})$  to oxidize organics and active  
453 chlorine, thus becoming much more effective to remove  $\text{NO}_3^-$ . Fig.7e reveals the accumulation of  
454 much greater contents of active chlorine as compared to the BDD/Fe cell, up to  $322 \text{ mg dm}^{-3}$  as

455 maximal, which decreased more largely as  $I$  grew up. The decay of active chlorine is due to its  
456 oxidation to  $\text{ClO}_3^-$  ion, which is generated to larger extent at higher  $I$ , as can be seen in Fig. 7f.

457 Regarding the TBZE abatement using the  $\text{RuO}_2$  anode, two tendencies can be observed in Fig.  
458 7a, as compared to the BDD/Fe cell: (i) a lower degradation rate at 250 and 500 mA, with the  
459 herbicide being mainly oxidized by  $\text{RuO}_2(\bullet\text{OH})$ , and (ii) a similar degradation at 1000 mA, when  
460 larger amounts of active chlorine act as pre-eminent oxidant. The change of  $k(\text{TBZE})$  between these  
461 two regions can be seen in Table 2. It can also be deduced that the best abatements were achieved at  
462 pH 4.0, regardless of the applied  $I$ . The greater production of active chlorine with  $\text{RuO}_2$  favors the  
463 overall oxidation of  $\text{NH}_3$  (not detected) to regenerate more  $\text{NO}_3^-$  ion at long electrolysis time. This  
464 can be inferred by comparing the  $\text{NO}_3^-$  profiles of Fig. 7b using  $\text{RuO}_2$  with those of Fig. 6b using  
465 BDD. However, the  $k(\text{NO}_3^-)$  values of Table 2 are greater for the  $\text{RuO}_2$  anode. This is not surprising  
466 because they were only determined during the first 60 min of electrolysis, because at higher time the  
467  $\text{NO}_3^-$  concentration in the medium was practically stabilized due to its fast regeneration from reaction  
468 (9). This phenomenon was not found with the BDD anode, where the  $\text{NO}_3^-$  concentration decayed  
469 gradually and excellent linear  $\ln([\text{NO}_3^-]_0/[\text{NO}_3^-])$  vs.  $t$  plots were obtained up to 300 min of  
470 electrolysis. In the same context, Fig. 7c shows a slower TN abatement using  $\text{RuO}_2$  than that obtained  
471 with BDD (see Fig. 6c). Despite this, high percentages of generated volatile N-compounds were  
472 always determined, as highlights Fig. 7d, corroborating again the fast reaction (8) to produce  $\text{N}_2$  gas.  
473 The main species in final solutions was the residual  $\text{NO}_3^-$  ion under all operation conditions. No  
474 combined chlorine forming chloramines was detected in both cells at the end of any experiment. This  
475 suggests that, if produced, they reacted rapidly either with the  $\text{NO}_2^-$  ion generated from reaction (1)  
476 according to reaction (15), or with the active chlorine present in solution to be oxidized to nitrate.



478 *3.4. Electrochemical oxidation/electrodenitrification process in softened actual groundwater*

479 Since the cell equipped with BDD yields faster EO and electrodenitrification than that with RuO<sub>2</sub>  
480 in chloride matrices, BDD/Fe cells were chosen to study the paired treatment of 5.0 mg dm<sup>-3</sup> TBZE  
481 spiked into actual softened groundwater (100 mg dm<sup>-3</sup> NO<sub>3</sub><sup>-</sup>) conditioned at pH 4.0. One cell had one  
482 Fe cathode and was operated at  $I = 500$  mA, whereas another cell had two Fe cathodes sandwiching  
483 the BDD anode to work at  $I = 1000$  mA. Moreover, to clarify the influence of NOM on the  
484 performance of the system, an assay with the latter cell was carried out with the simulated chloride  
485 matrix. A significant effect of using two Fe cathodes instead of one at 1000 mA was the notable decay  
486 of  $E_{\text{cell}}$  (8.8 V vs 14.7 V), giving rise to a great reduction of EC (105.6 kWh m<sup>-3</sup> vs. 176.4 kWh m<sup>-3</sup>)  
487 (see Table 2). Therefore, the number and position of the electrodes plays a crucial role in the  
488 optimization of the energy parameters. In contrast, final pH values close to 10.5 were always obtained  
489 at the end of the treatment for both systems.

490 A similar TBZE content decay can be observed in Fig. 8a for the simulated and actual softened  
491 groundwater using two Fe anodes, achieving the total removal in 40 min, which suggests that the  
492 influence of NOM oxidation was irrelevant. In fact, Table 2 shows that the  $k(\text{TBZE})$  value for both  
493 treatments (about 0.16 min<sup>-1</sup>) was even greater than 0.10 and 0.12 min<sup>-1</sup> determined for the cell with  
494 one Fe cathode at 500 mA (i.e., the same current density than using two Fe cathodes at 1000 mA) and  
495 1000 mA, thus being the TBZE degradation faster and more efficient. In contrast, Fig. 8b depicts a  
496 slower destruction of the intermediate DE-TBZE in the actual groundwater after reaching a maximal  
497 of 0.26 mg dm<sup>-3</sup>, which can be ascribed to the loss of oxidizing agents that are partly consumed by  
498 NOM. The effect of the organic matter was also evaluated for the evolution of NO<sub>3</sub><sup>-</sup>, NH<sub>4</sub><sup>+</sup> and TN.  
499 Fig. 8c and 8e show a very fast NO<sub>3</sub><sup>-</sup> and TN decay in the simulated groundwater with two Fe  
500 cathodes, much more rapid than using one Fe cathode at the same  $I$  (see Fig. 6b and 6c). These figures  
501 also show a strong inhibition of both parameters in the actual groundwater, which can be explained  
502 by the fouling effect of NOM and residual Mg on the cathode surface and a small formation of NO<sub>3</sub><sup>-</sup>  
503 ion from the degradation of NOM. This influence of the organic matter was also evident for the NO<sub>3</sub><sup>-</sup>

504 content removal when using the cell with one Fe cathode at  $I = 500$  mA to treat the actual groundwater  
505 (see Fig. 8c), but it was irrelevant for TN decay as compared to the trial with two Fe cathodes (see  
506 Fig. 8e). Fig. 8d reveals the expected greater accumulation of  $\text{NH}_4^+$  ion in the three treatments as a  
507 greater  $\text{NO}_3^-$  concentration was abated.

508 A different behavior was observed for the time course of  $\text{Cl}^-$ ,  $\text{ClO}_3^-$  and  $\text{ClO}_4^-$  ions, mainly  
509 depending on the applied  $I$  and with little influence of the number of Fe cathodes, as can be seen in  
510 Fig. 8f-8h. Total  $\text{Cl}^-$  removal was reached in 240 min using two Fe cathodes, with similar  $k(\text{Cl}^-)$   
511 values of  $1.32\text{-}1.40 \times 10^{-2} \text{ min}^{-1}$ , very close to  $1.24 \times 10^{-2} \text{ min}^{-1}$  determined with one Fe cathode (see  
512 Table 2). The lower  $I$  of 500 mA with two Fe cathodes yielded an 88% reduction of  $\text{Cl}^-$  content in  
513 360 min, with  $k(\text{Cl}^-) = 5.7 \times 10^{-3} \text{ min}^{-1}$ , slightly lower than  $7.5 \times 10^{-3} \text{ min}^{-1}$  found with one Fe cathode  
514 (see Table 2). All the active chlorine produced from  $\text{Cl}^-$  oxidation was then transformed into  $\text{ClO}_3^-$ ,  
515 which was converted into  $\text{ClO}_4^-$ , to larger extent at higher  $I$ . For the actual groundwater at  $I = 1000$   
516 mA,  $59 \text{ mg dm}^{-3}$  of  $\text{ClO}_3^-$  and  $767 \text{ mg dm}^{-3}$  of  $\text{ClO}_4^-$  were finally obtained. The latter content was  
517 smaller than  $975 \text{ mg dm}^{-3}$  determined in the simulated groundwater, which can be due to the loss of  
518 active chlorine by reaction with the organic matter. The  $\text{ClO}_3^-$  and  $\text{ClO}_4^-$  concentrations after  
519 electrolysis of the actual groundwater need to be removed before disposal or reuse. Aiming at  
520 evaluating the viability of the technology for future scale-up, a post-treatment was applied by  
521 employing a commercial ion-exchange resin. Table 1 shows that this resin allowed the overall  
522 removal of  $\text{ClO}_4^-$  and  $\text{NO}_2^-$  anions, most of the residual  $\text{ClO}_3^-$  ion and partial removal of  $\text{NO}_3^-$  and  
523  $\text{SO}_4^{2-}$  ions.

### 524 3.5. Identification of heteroaromatic byproducts and proposal of initial reaction sequence

525 Table 3 summarizes the chemical name, molecular structure, type of column, retention time and  
526 fragments for the stable heteroaromatic byproducts of TBZE (**1**) identified after 60 min of electrolysis  
527 of simulated matrices with and without chloride containing  $5.0 \text{ mg dm}^{-3}$  herbicide. For this, the

528 BDD/Fe tank reactor was operated at  $I = 500$  mA. Although different byproducts were identified in  
529 each medium due to the different oxidation environments, any organochlorine derivative was found  
530 despite the formation and attack of active chlorine in the chloride matrix, as pointed out above. This  
531 surprising finding can be explained by the rapid destruction of such chloro-compounds by the strong  
532 oxidant BDD( $\bullet$ OH). As can be seen in Table 3, ten heteroaromatics were identified related to: (i) the  
533 release of either the Cl atom with hydrogenation (compound **2**) or hydroxylation (compound **3**), the  
534 lateral ethyl group (compound **4**), the lateral *tert*-butyl group (compound **6**) or both lateral groups  
535 (compound **10**); (ii) the carbonylation of the ethyl group (compounds **5**, **8** and **9**); (iii) the oxidation  
536 of the *tert*-butyl group (compound **7**); and (iv) the overall hydroxylation (compound **11**) of these  
537 products. Note that compounds **4-6** have been previously reported by other authors for **1** degradation  
538 [52,57]. Compounds **4** (DE-TBZE) and **11** (cyanuric acid) have been also detected and quantified in  
539 this work by reversed-phase and ion-exclusion HPLC, respectively.

540 Based on the identified heteroaromatics, an initial route for **1** destruction by EO with a BDD  
541 anode is proposed in Fig. 9. In this pathway, BDD( $\bullet$ OH) is assumed as the main oxidant. The initial  
542 attack of this radical over **1** leads to 5 compounds: (i) **2** with hydrogenation and Cl loss, (ii) **3** with  
543 hydroxylation and Cl release, (iii) **4** with release of the ethyl group, (iv) **5** with carbonylation of the  
544 ethyl group and (v) **6** with loss of the *tert*-butyl group. The subsequent release of the ethenyl group  
545 with oxidation of the *tert*-butyl group of **3** yields **7**, whereas the hydroxylation of **5** gives **8** and the  
546 carbonylation of **6** produces **9**. Transformation of **5** and **8** into **4**, as well as that of **5** into **9**, is feasible.  
547 Compounds **4-6**, **8** and **9** can then evolve to **10** and all products to **11** as final heteroaromatic.

#### 548 **4. Conclusions**

549 This study has presented a comprehensive set of EO, electroreduction and EO/electroreduction trials  
550 in simulated and actual groundwater matrices with only  $\text{NO}_3^-$ , only TBZE or  $\text{NO}_3^- + \text{TBZE}$ , in the  
551 absence and presence of  $\text{Cl}^-$ . The BDD/Fe and  $\text{RuO}_2/\text{Fe}$  cells showed a very high effectiveness to

552 simultaneously remove nitrate and pesticide from the solutions. From our results, it can be concluded  
553 that an effective treatment of groundwater polluted with nitrate and TBZE pesticide requires a  
554 sequence of three steps: (i) Softening to minimize the  $\text{Ca}^{2+}$  and  $\text{Mg}^{2+}$  content that block the  
555 electrocatalytic nitrate electroreduction; (ii) EO/electrodenitrification with a BDD/Fe or  $\text{RuO}_2/\text{Fe}$  cell,  
556 preferably with two Fe cathode because the greater exposed surface favored the occurrence of  
557 electrocatalysis; and (iii) post-treatment with an anion-exchange resin to minimize the chlorate and  
558 perchlorate concentrations and achieve an additional nitrate removal. The NOM contained in the  
559 groundwater had no negative influence on TBZE removal, but it decelerated the nitrate removal. All  
560 removals became faster as the applied current was increased from 250 to 1000 mA. Once  
561 demonstrated that the paired electrolysis of nitrate + pesticide solutions can be highly effective with  
562 BDD/Fe and  $\text{RuO}_2/\text{Fe}$  cells at small scale, further work is being carried out in our laboratory to scale-  
563 up the treatment using a flow reactor.

#### 564 **Acknowledgements**

565 The authors thank the financial support from project PID2019-109291RB-I00 (AEI, Spain). R.  
566 Oriol acknowledges the FPI grant awarded by MINECO (Spain).

#### 567 **References**

- 568 [1] M. Gutiérrez, R.N. Biagioni, M.T. Alarcón-Herrera, B.A. Rivas-Lucero, An overview of nitrate  
569 sources and operating processes in arid and semiarid aquifer systems, *Sci. Total Environ.* 624  
570 (2018) 1513–1522.
- 571 [2] M. Duca, M.T.M. Koper, Powering denitrification: the perspectives of electrocatalytic nitrate  
572 reduction, *Energy Environ. Sci.* 5 (2012) 9726–9742.
- 573 [3] M. Zhou, W. Fu, H. Gu, L. Lei, Nitrate removal from groundwater by a novel three-dimensional  
574 electrode biofilm reactor, *Electrochim. Acta* 52 (2007) 6052–6059.



- 575 [4] M. Shrimali, K.P. Singh, J. Greeley, New methods of nitrate removal from water, *Environ. Poll.*  
576 112 (2001) 351–359.
- 577 [5] M. Li, C. Feng, Z. Zhang, X. Lei, R. Chen, Y. Yang, N. Sugiura, Simultaneous reduction of  
578 nitrate and oxidation of by-products using electrochemical method, *J. Hazard. Mater.* 171  
579 (2009) 724–730.
- 580 [6] H. Cheng, K. Scott, P.A. Christensen, Paired electrolysis in a solid polymer electrolyte reactor-  
581 simultaneously reduction of nitrate and oxidation of ammonia, *Chem. Eng. J.* 108 (2005) 257–  
582 268.
- 583 [7] H. Cheng, K. Scott, P.A. Christensen, Application of a solid polymer electrolyte reactor to  
584 remove nitrate ions from wastewater, *J. Appl. Electrochem.* 35 (2005) 551–560.
- 585 [8] I. Katsounaros, G. Kyriacou, Influence of the concentration and the nature of the supporting  
586 electrolyte on the electrochemical reduction on tin cathode, *Electrochim. Acta* 52 (2007) 6412–  
587 6420.
- 588 [9] I. Katsounaros, G. Kyriacou, Influence of nitrate concentration on its electrochemical reduction  
589 on tin cathode: identification of reaction intermediates, *Electrochim. Acta* 53 (2008) 5477–  
590 5484.
- 591 [10] D. Reyter, D. Bélanger, L. Roué, Study of the electroreduction of nitrate on copper in alkaline  
592 solution, *Electrochim. Acta* 53 (2008) 5977–5984.
- 593 [11] W. Huang, M. Li, B. Zhang, C. Feng, X., Lei, B. Xu, Influence of operating conditions on  
594 electrochemical reduction of nitrate in groundwater, *Water Environ. Res.* 85 (2013) 224–231.
- 595 [12] M. Li, C. Feng, Z. Zhang, Z. Shen, N. Sugiura, Electrochemical reduction of nitrate using  
596 various anodes and a Cu/Zn cathode, *Electrochem. Commun.* 11 (2009) 1853–1856.
- 597 [13] B. Talhi, F. Monette, A. Azzouz, Effective and selective nitrate electroreduction into nitrogen  
598 through synergistic parameter interactions, *Electrochim. Acta* 58 (2011) 276–284.

- 599 [14] R. Oriol, M.P. Bernícola, E. Brillas, P.L. Cabot, I. Sirés, Paired electrooxidation of insecticide  
600 imidacloprid and electrodenitrification in simulated and real water matrices, *Electrochim. Acta*  
601 317 (2019) 753–765.
- 602 [15] E. Lacasa, P. Cañizares, J. Llanos, M.A. Rodrigo, Effect of the cathode material on the removal  
603 of nitrates by electrolysis in non-chloride media, *J. Hazard. Mater.* 213-214 (2012) 478–484.
- 604 [16] E. Lacasa, J. Llanos, P. Cañizares, M.A. Rodrigo, Electrochemical denitrification with  
605 chlorides using DSA and BDD anodes, *Chem. Eng. J.* 184 (2012) 66–71.
- 606 [17] M. Dortsiu, I. Katsounaros, C. Polatides, G. Kyriacou, Influence of the electrode and the pH on  
607 the rate and the product distribution of the electrochemical removal of nitrate, *Environ. Technol.*  
608 34 (2013) 373–381.
- 609 [18] Y.Y. Birdja, J. Yang, M.T.M. Koper, Electrocatalytic reduction of nitrate on tin-modified  
610 palladium electrodes, *Electrochim. Acta* 140 (2014) 518–524.
- 611 [19] L. Rajic, D. Berroa, S. Gregor, S. Elbakri, M. MacNeil, A.N. Alshawabkeh, Electrochemically-  
612 induced reduction of nitrate in aqueous solution, *Int. J. Electrochem. Sci.* 12 (2017) 5998–6009.
- 613 [20] C. Sun, F. Li, H. An, Z. Li, A.M. Bond, J. Zhang, Facile electrochemical co-deposition of metal  
614 (Cu, Pd, Pt, Rh) nanoparticles on reduced graphene oxide for electrocatalytic reduction of  
615 nitrate/nitrite, *Electrochim. Acta* 269 (2018) 733–741.
- 616 [21] Y. Zhang, Y. Zhao, Z. Chen, L. Wang, P. Wu, F. Wang, Electrochemical reduction of nitrate  
617 via Cu/Ni composite cathode paired with Ir-Ru/Ti anode: high efficiency and N<sub>2</sub> selectivity,  
618 *Electrochim. Acta* 291 (2018) 151–160.
- 619 [22] L. Wu, Y. Shi, C. Su, H. Cao, G. Zheng, Efficient electrochemical reduction of high  
620 concentration nitrate by a stepwise method, *Catal. Lett.* 149 (2019) 1216–1223.
- 621 [23] D.E. Kim, D. Pak, Ti plate with TiO<sub>2</sub> nanotube arrays as a novel cathode for nitrate reduction,  
622 *Chemosphere* 228 (2019) 611–618.

- 623 [24] I. Sanjuán, L. García-Cruz, J. Solla-Gullón, E. Expósito, V. Montiel, Bi-Sn nanoparticles for  
624 electrochemical denitrification: activity and selectivity towards N<sub>2</sub> formation, *Electrochim.*  
625 *Acta* 340 (2020) 135914.
- 626 [25] J. Martínez, A. Ortiz, I. Ortiz, State-of-the-art and perspectives of the catalytic and  
627 electrocatalytic reduction of aqueous nitrates, *Appl. Catal. B: Environ.* 207 (2017) 42–59.
- 628 [26] J.R. Steter, E. Brillas, I. Sirés, On the selection of the anode material for the electrochemical  
629 removal of methylparaben from different aqueous media, *Electrochim. Acta* 222 (2016) 1464–  
630 1474.
- 631 [27] S. Lanzalaco, I. Sirés, A. Galia, M.A. Sabatino, C. Dispenza, O. Scialdone, Facile crosslinking  
632 of poly(vinylpyrrolidone) by electro-oxidation with IrO<sub>2</sub>-based anode under potentiostatic  
633 conditions, *J. Appl. Electrochem.* 48 (2018) 1343–1352.
- 634 [28] G. Daniel, Y. Zhang, S. Lanzalaco, F. Brombin, T. Kosmala, G. Granozzi, A. Wang, E. Brillas,  
635 I. Sirés, C. Durante, Chitosan-derived nitrogen-doped carbon electrocatalyst for a sustainable  
636 upgrade of oxygen reduction to hydrogen peroxide in UV-assisted electro-Fenton water  
637 treatment, *ACS Sustain. Chem. Eng.* 8 (2020) 14425–14440.
- 638 [29] R. Oriol, D. Clematis, E. Brillas, J.L. Cortina, M. Panizza, I. Sirés, Groundwater treatment using  
639 a solid polymer electrolyte cell with mesh electrodes, *ChemElectroChem* 6 (2019) 1235–1243.
- 640 [30] L. Li, Y. Liu, Ammonia removal in electrochemical oxidation: mechanism and pseudo-kinetics,  
641 *J. Hazard. Mater* 161 (2009) 1010–1016.
- 642 [31] G. Pérez, J. Saiz, R. Ibañez, A.M. Urtiaga, I. Ortiz, Assessment of the formation of inorganic  
643 oxidation by-products during the electrocatalytic treatment of ammonium from landfill  
644 leachates, *Water Res.* 46 (2012) 2579–2590.
- 645 [32] C. Zhang, D. He, J. Ma, D. Waite, Active chlorine mediated ammonia oxidation revisited:  
646 reaction mechanism, kinetic modelling and implications, *Water Res.* 145 (2018) 220–230.

- 647 [33] P. Mandal, M.K. Yadav, A.K. Gupta, B.K. Dubey, Chlorine mediated indirect electro-oxidation  
648 of ammonia using non-active  $\text{PbO}_2$  anode: influencing parameters and mechanism  
649 identification, *Sep. Purif. Technol.* 247 (2020) 116910.
- 650 [34] D.G. Wahman, G.E. Speitel Jr, Relative importance of nitrite oxidation by hypochlorous acid  
651 under chloramination conditions, *Environ. Sci. Technol.* 46 (2012) 6056–6064.
- 652 [35] J. Chen, H. Shi, J. Lu, Electrochemical treatment of ammonia in wastewater by  $\text{RuO}_2\text{-IrO}_2\text{-}$   
653  $\text{TiO}_2/\text{Ti}$  electrodes, *J. Appl. Electrochem.* 37 (2007) 1137–1144.
- 654 [36] A. Kapalka, A. Katsaounis, N.L. Michels, A. Leonidova, S. Souentie, C. Comninellis, K.M.  
655 Udert, Ammonia oxidation to nitrogen mediated by electrogenerated active chlorine on  
656  $\text{Ti/PtOx-IrO}_2$ , *Electrochem. Commun.* 12 (2010) 1203–1205.
- 657 [37] I. Sirés, E. Brillas, G. Cerisola, M. Panizza, Comparative depollution of mecoprop aqueous  
658 solutions by electrochemical incineration using BDD and  $\text{PbO}_2$  as high oxidation power anodes,  
659 *J. Electroanal. Chem.* 613 (2008) 151–159.
- 660 [38] A.R.F. Pipi, I. Sirés, A.R. De Andrade, E. Brillas, Application of electrochemical advanced  
661 oxidation processes to the mineralization of the herbicide diuron, *Chemosphere* 109 (2014) 49–  
662 55.
- 663 [39] F. Gozzi, I. Sirés, A. Thiam, S.C. de Oliveira, A. Machulek Jr., E. Brillas, Treatment of single  
664 and mixed pesticide formulations by solar photoelectro-Fenton using a flow plant, *Chem. Eng.*  
665 *J.* 310 (2017) 503–513.
- 666 [40] D.R.V. Guelfi, F. Gozzi, A. Machulek Jr., I. Sirés, E. Brillas, S.C. de Oliveira, Degradation of  
667 herbicide S-metolachlor by electrochemical AOPs using a boron-doped diamond anode, *Catal.*  
668 *Today* 313 (2018) 182–188.
- 669 [41] D.R.V. Guelfi, E. Brillas, F. Gozzi, A. Machulek Jr., S.C. de Oliveira, I. Sirés, Influence of  
670 electrolysis conditions on the treatment of herbicide bentazon using artificial UVA radiation  
671 and sunlight. Identification of oxidation products, *J. Environ. Manage.* 231 (2019) 213–221.

- 672 [42] D.R.V. Guelfi, Z. Ye, F. Gozzi, S.C. de Oliveira, A. Machulek Jr., E. Brillas, I. Sirés, Ensuring  
673 the overall combustion of herbicide metribuzin by electrochemical advanced oxidation  
674 processes. Study of operation variables, kinetics and degradation routes, *Sep. Purif. Technol.*  
675 211 (2019) 637–645.
- 676 [43] A.L. Tasca, M. Puccini, A. Fletcher, Terbutylazine and desethylterbutylazine: recent  
677 occurrence, mobility and removal techniques, *Chemosphere* 202 (2018) 94–104.
- 678 [44] P. Bottoni, P. Grenni, L. Lucentini, A. Barra Caracciolo, Terbutylazine and other triazines in  
679 Italian water resources, *Microchem. J.* 108 (2013) 136–142.
- 680 [45] E. Drazevic, K. Kosutic, S. Fingler, V. Drevenkar, Removal of pesticides from the water and  
681 their adsorption on the reverse osmosis membranes of defined porous structure, *Des. Water*  
682 *Treat.* 1-3 (2011) 161–170.
- 683 [46] S. Ronka, M. Kujawska, H. Jusiewicz, Triazines removal by selective polymeric adsorbent,  
684 *Pure Appl. Chem.* 11 (2014) 1755–1769.
- 685 [47] P.M. Álvarez, D.H. Quiñones, I. Terrones, A. Rey, F.J. Beltrán, Insights into the removal of  
686 terbutylazine from aqueous solution by several treatment methods, *Water Res.* 98 (2016) 334–  
687 343.
- 688 [48] L. Liang, X. Wang, Y. Sun, P. Ma, X. Li, H. Piao, Y. Jiang, D. Song, Magnetic solid-phase  
689 extraction of triazine herbicides from rice using metal-organic framework MIL-101(Cr)  
690 functionalized magnetic particles, *Talanta* 179 (2018) 512–519.
- 691 [49] S. Sorlini, F. Gialdini, M. Stefan, UV/H<sub>2</sub>O<sub>2</sub> oxidation of arsenic and terbutylazine in drinking  
692 water, *Environ. Monit. Assess.* 186 (2014) 1311–1316.
- 693 [50] A.F. Tchicaya, S.B. Wognin, I.A.A. Aka, Y.M. Kouassi, A.L.M. N'Guessan, Photocatalytic  
694 degradation of the herbicide terbutylazine: preparation, characterization and photoactivity of  
695 the immobilized thin layer of TiO<sub>2</sub>/chitosan, *J. Photochem. Photobiol. A* 309 (2015) 22–29.

- 696 [51] D.H. Quiñones, A. Rey, P.M. Álvarez, F.J. Beltrán, G.L. Puma, Boron doped TiO<sub>2</sub> catalysts for  
697 photocatalytic ozonation of aqueous mixtures of common pesticides: diuron, o-phenylphenol,  
698 MCPA and terbuthylazine, *Appl. Catal. B: Environ.* 178 (2015) 74–81.
- 699 [52] A.L. Tasca, M. Puccini, D. Clematis, M. Panizza, Electrochemical removal of terbuthylazine:  
700 boron-doped diamond anode coupled with solid polymer electrolyte, *Environ. Pollut.* 251  
701 (2019) 285–291.
- 702 [53] APWA, AWWA, WEF, *Standard Methods for the Examination of Water and Wastewater*, 21st  
703 ed., Method Number 4500-Cl Chlorine (residual)–G. DPD Colorimetric Method, American  
704 Public Health Association, Washington D.C., 2005, pp. 4-67 and 4–68.
- 705 [54] A. Thiam, I. Sirés, J.A. Garrido, R.M. Rodríguez, E. Brillas, Effect of anions on electrochemical  
706 degradation of azo dye Carmoisine (Acid Red 14) using a BDD anode and air-diffusion cathode,  
707 *Sep. Purif. Technol.* 140 (2015) 43–52.
- 708 [55] J.R. Steter, E. Brillas, I. Sirés, Solar photoelectro-Fenton treatment of a mixture of parabens  
709 spiked into secondary treated wastewater effluent at low input current, *Appl. Catal. B: Environ.*  
710 224 (2018) 410–418.
- 711 [56] N. Borràs, R. Oliver, C. Arias, E. Brillas, Degradation of atrazine by electrochemical advanced  
712 oxidation process using boron-doped diamond anode, *J. Phys. Chem.* 114 (2010) 6613–6621.
- 713 [57] S.V. Pereira, T. Reis, B.S. Souza, R.F. Dantas, D.A. Azevedo, M. Dezotti, C. Sans, S. Esplugas,  
714 Oestrogenicity assessment of s-triazines by products during ozonation, *Environ. Technol.* 36  
715 (2014) 1-25.
- 716

717 **Figure captions**

718 **Fig. 1.** (a)  $\text{NO}_3^-$  concentration removal during the electrodenitrification of  $500 \text{ cm}^3$  of a solution  
719 containing  $100 \text{ mg dm}^{-3} \text{NO}_3^- + 7.6 \text{ mM SO}_4^{2-}$  in ultrapure water at initial pH 4.0, 7.0 and 10.5, using  
720 undivided stirred BDD/Fe or  $\text{RuO}_2/\text{Fe}$  tank reactors at 500 mA and  $25 \text{ }^\circ\text{C}$ . (b) Pseudo-first-order  
721 kinetic analysis of trends of plot (a), (c) accumulated  $\text{NH}_4^+$  contents, (d) normalized total nitrogen  
722 decays, and (e) percent distributions of the nitrogen species at the end of the trials.

723 **Fig. 2.** (a)  $\text{NO}_3^-$  content decay during the electrodenitrification of  $500 \text{ cm}^3$  of a solution containing  
724  $10 \text{ mM Cl}^- + 100 \text{ mg dm}^{-3} \text{NO}_3^- + 0.8 \text{ mM SO}_4^{2-}$  in ultrapure water at different pH values, using  
725 undivided stirred BDD/Fe or  $\text{RuO}_2/\text{Fe}$  tank reactors at several  $I$  values and  $25 \text{ }^\circ\text{C}$ . (b) Pseudo-first-  
726 order kinetic analysis of trends of plot (a), (c) N accumulated  $\text{NH}_4^+$  contents, (d) normalized total  
727 nitrogen decays, and (e) percent distributions of the nitrogen species at the end of the trial at  $I = 500$   
728 mA.

729 **Fig. 3.** Change of the concentrations of (a)  $\text{Cl}^-$  ion ( $355 \text{ mg dm}^{-3}$  of initial  $\text{Cl}^-$ ), (c)  $\text{ClO}_3^-$  ion, and (d)  
730  $\text{ClO}_4^-$  ion with electrolysis time for the assays of Fig. 2. (b) Pseudo first-order kinetic analysis for the  
731 data of plot (a).

732 **Fig. 4.** (a) Time course of terbuthylazine (TBZE) concentration and its pseudo-first-order decay  
733 (inset) during the electrochemical oxidation (EO) of  $500 \text{ cm}^3$  of a  $10 \text{ mM Na}_2\text{SO}_4$  solution with  $5 \text{ mg}$   
734  $\text{dm}^{-3}$  herbicide in pure water, using an undivided stirred BDD/Fe tank reactor at 500 mA and  $25 \text{ }^\circ\text{C}$ .  
735 The content of compounds accumulated during this trial is shown in: (b) desethyl-terbuthylazine (DE-  
736 TBZE), (c) inorganic N-compounds ( $\text{N-NH}_4^+$  and  $\text{N-NO}_3^-$ ) and (d) final acids.

737 **Fig. 5.** (a) TBZE content abatement during the paired EO/electrodenitrification of  $500 \text{ cm}^3$  of a  
738 solution containing  $5 \text{ mg dm}^{-3}$  herbicide in pure water with  $100 \text{ mg dm}^{-3} \text{NO}_3^- + 7.6 \text{ mM SO}_4^{2-}$  at pH  
739 4.0, using undivided stirred BDD/Fe or  $\text{RuO}_2/\text{Fe}$  tank reactors at 500 mA and  $25 \text{ }^\circ\text{C}$ . (b) Accumulated

740 DE-TBZE concentrations, (c)  $\text{NO}_3^-$  concentration removal, (d)  $\text{NH}_4^+$  accumulated concentrations, (e)  
741 normalized total nitrogen decays, and (f) percent distributions of the nitrogen compounds at the end  
742 of the trials.

743 **Fig. 6.** Influence of pH and current on the time course of (a) TBZE content during the paired  
744 EO/electrodenitrification of  $500 \text{ cm}^3$  of a solution containing  $5 \text{ mg dm}^{-3}$  herbicide in pure water with  
745  $10 \text{ mM Cl}^- + 100 \text{ mg dm}^{-3} \text{ NO}_3^- + 0.8 \text{ mM SO}_4^{2-}$ , using an undivided stirred BDD/Fe tank reactor at  
746  $25 \text{ }^\circ\text{C}$ . (b)  $\text{NO}_3^-$  concentrations, (c) normalized total nitrogen decays, (d) percent distribution of the  
747 nitrogen species at the end of the trials, (e) active chlorine concentrations, (f)  $\text{ClO}_3^-$  contents and (g)  
748  $\text{ClO}_4^-$  concentrations.

749 **Fig. 7.** Effect of pH and current under the conditions described in Fig. 6, but using an undivided  
750 stirred  $\text{RuO}_2/\text{Fe}$  tank reactor.

751 **Fig. 8.** Change of the concentrations of: (a) TBZE, (b) DE-TBZE, (c)  $\text{NO}_3^-$ , (d)  $\text{NH}_4^+$ , (e) normalized  
752 total nitrogen, (f)  $\text{Cl}^-$ , (g)  $\text{ClO}_3^-$  and (h)  $\text{ClO}_4^-$  during the paired EO/electrodenitrification of  $500 \text{ cm}^3$   
753 of the simulated groundwater ( $10 \text{ mM Cl}^- + 100 \text{ mg dm}^{-3} \text{ NO}_3^- + 0.8 \text{ mM SO}_4^{2-}$ ) or softened actual  
754 groundwater containing  $5 \text{ mg dm}^{-3}$  herbicide, using 1 BDD anode and 2 Fe cathodes. For comparison,  
755 the results for the treatment of actual groundwater without TBZE using 1 Fe cathode are also shown.

756 **Fig. 9.** Initial reaction pathway for terbuthylazine degradation in groundwater by EO with a BDD/Fe  
757 cell.



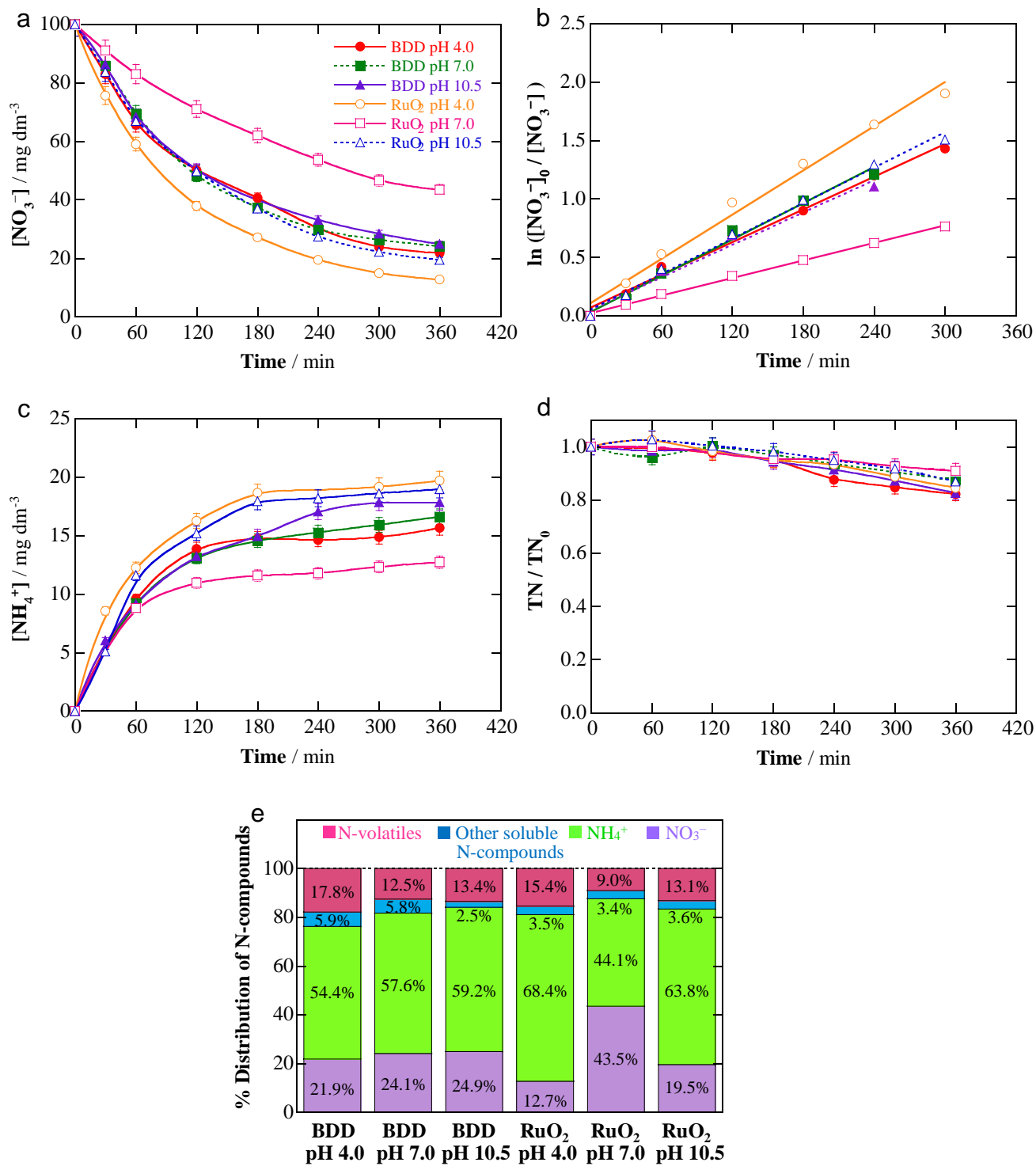
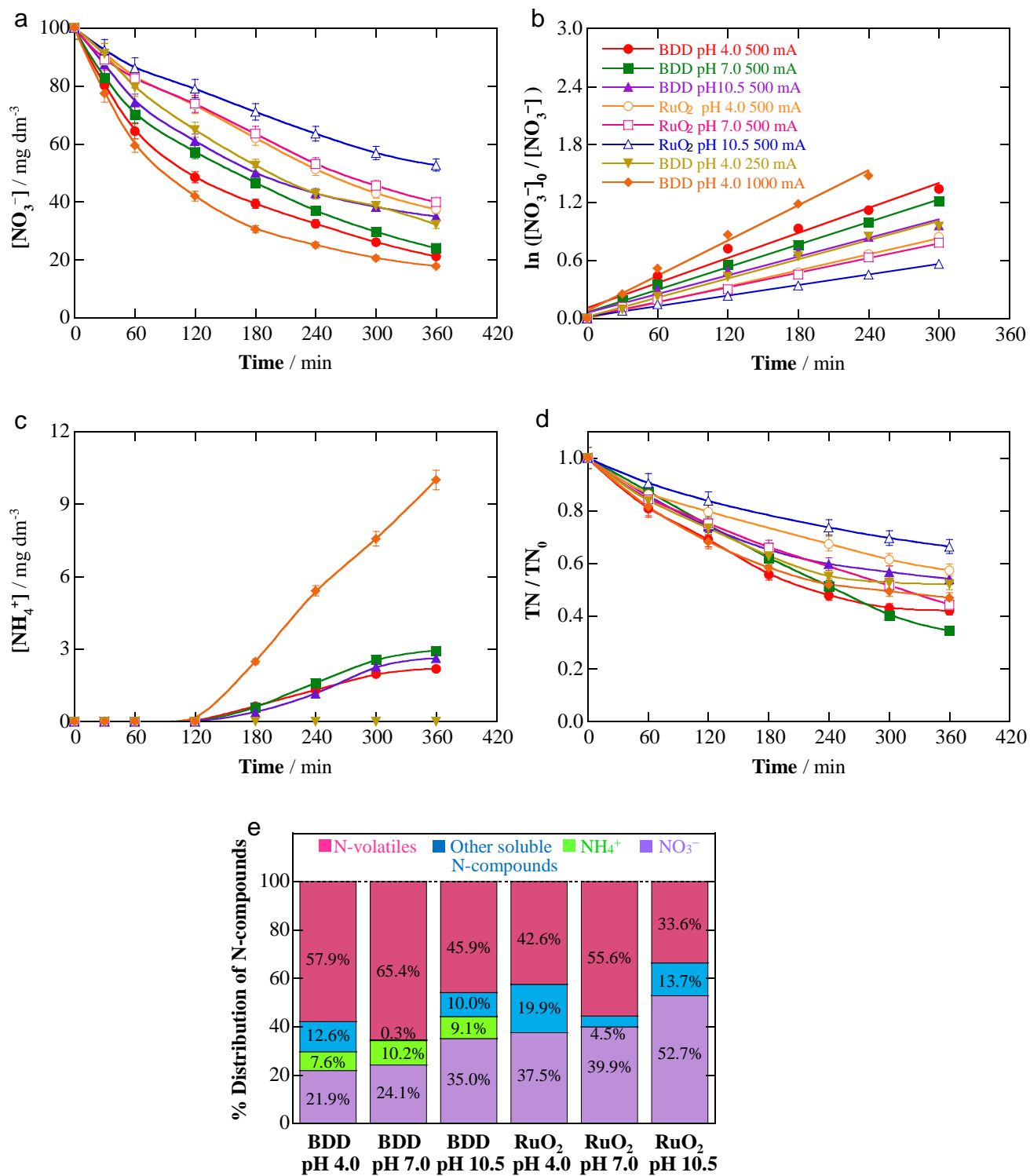
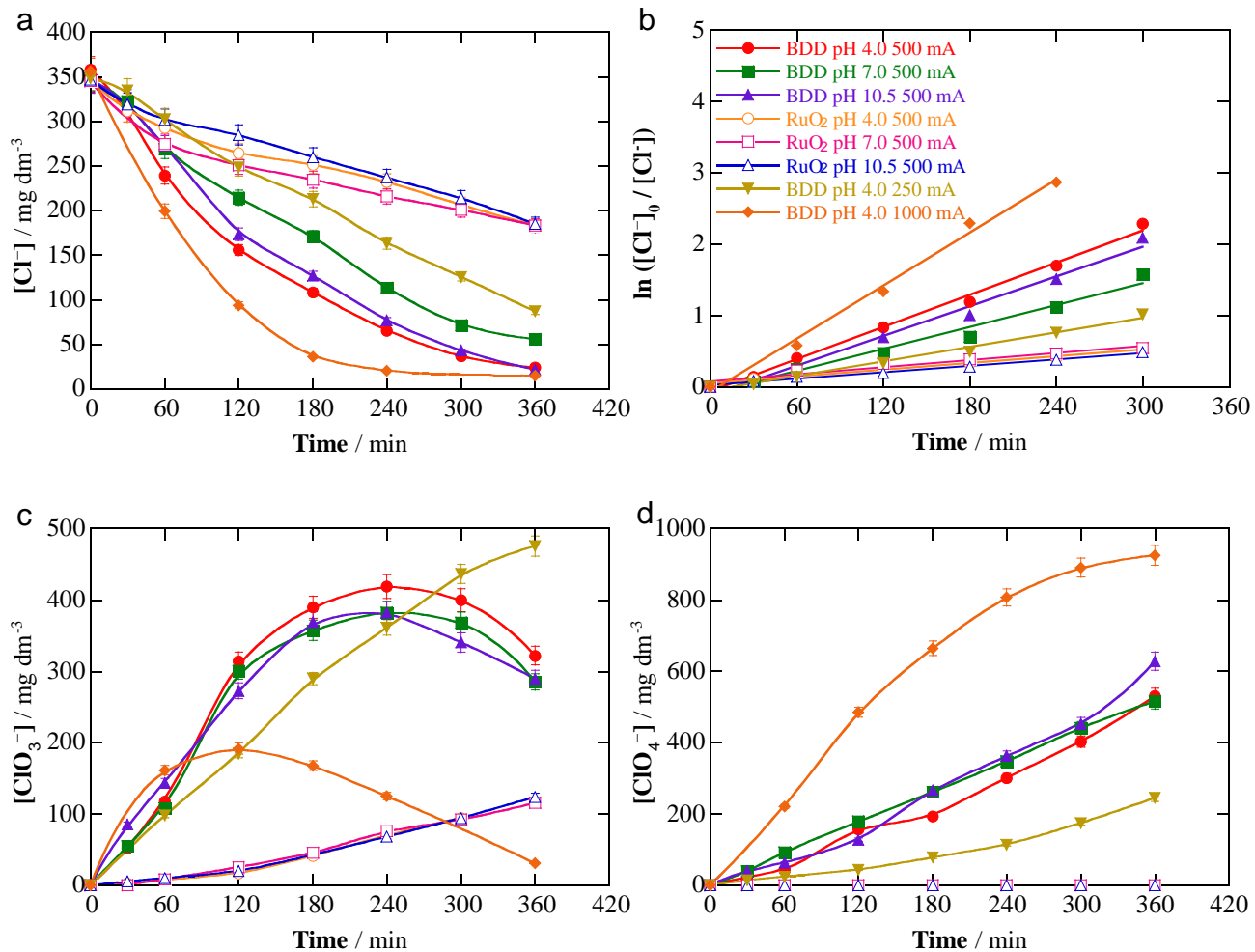


Fig. 1



**Fig. 2**



**Fig. 3**

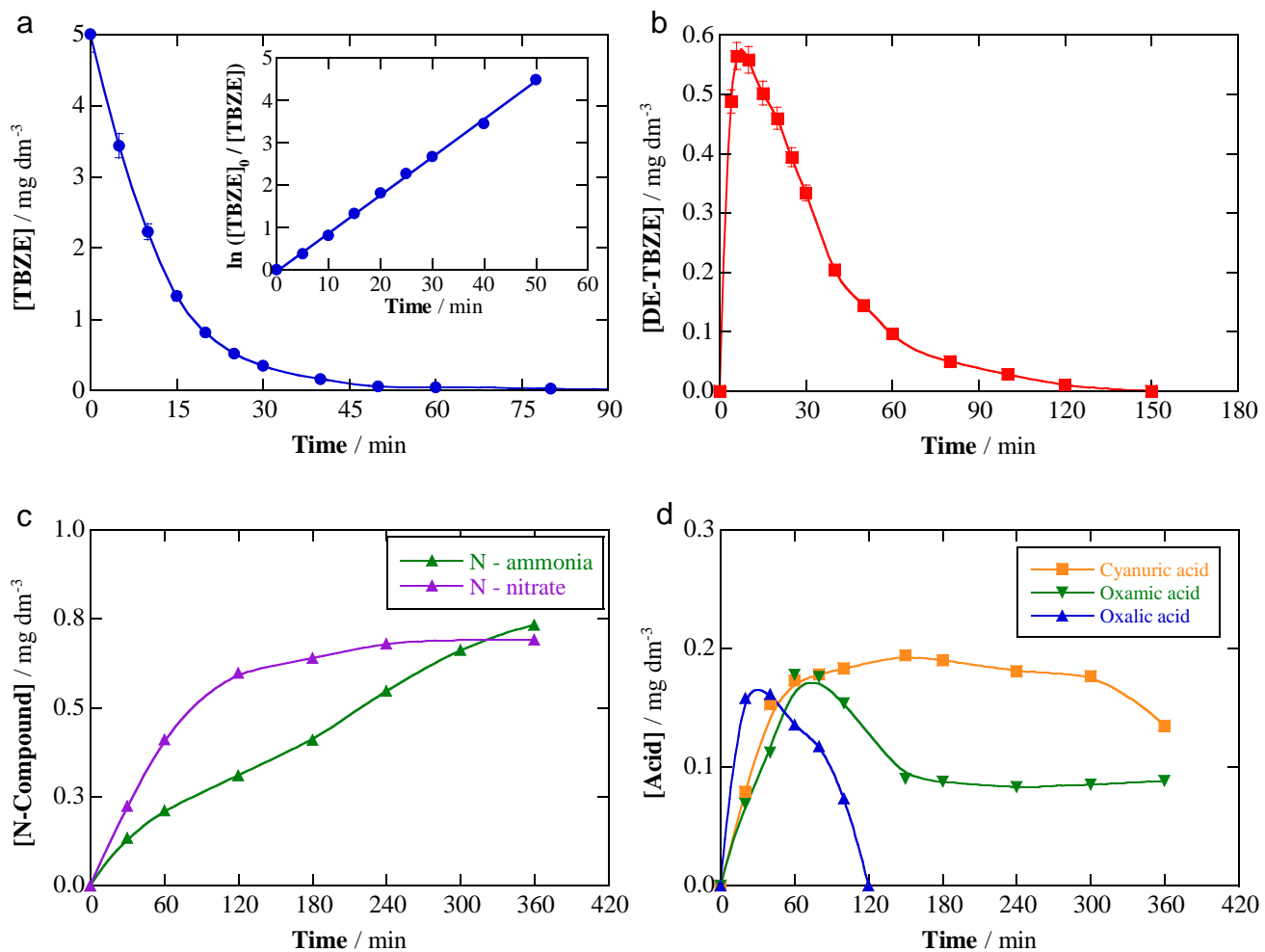


**Fig. 4**

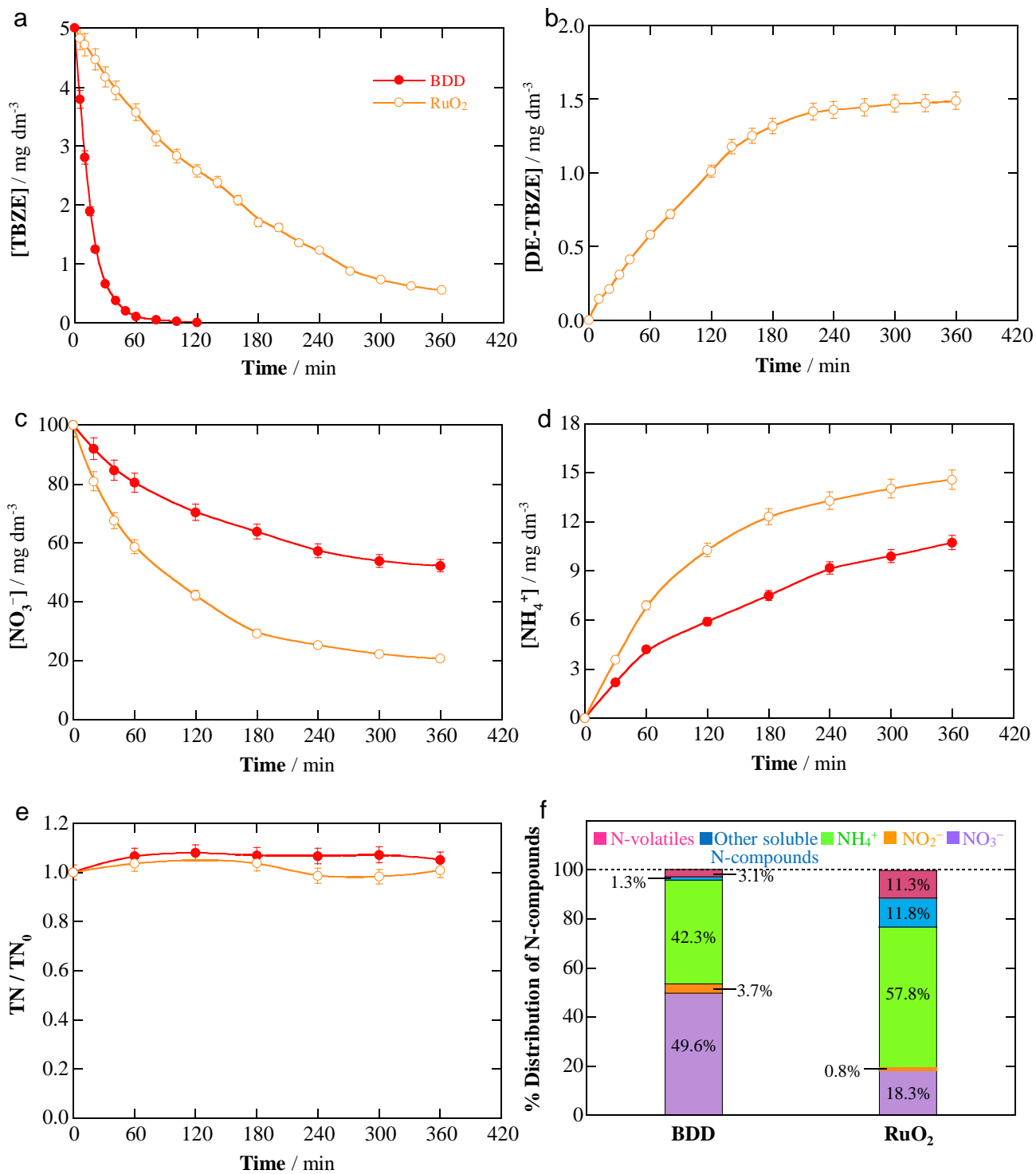


**Fig. 5**

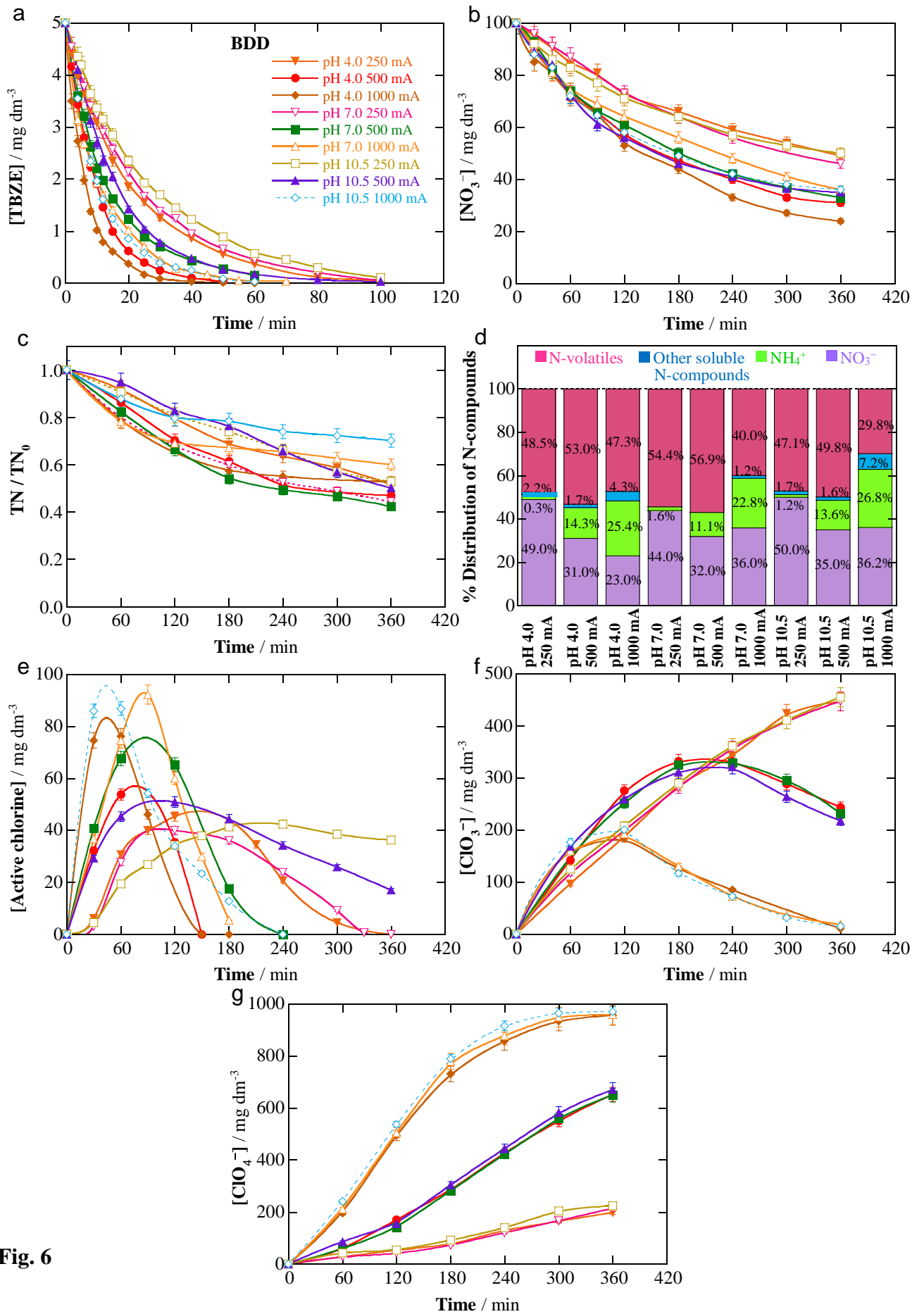
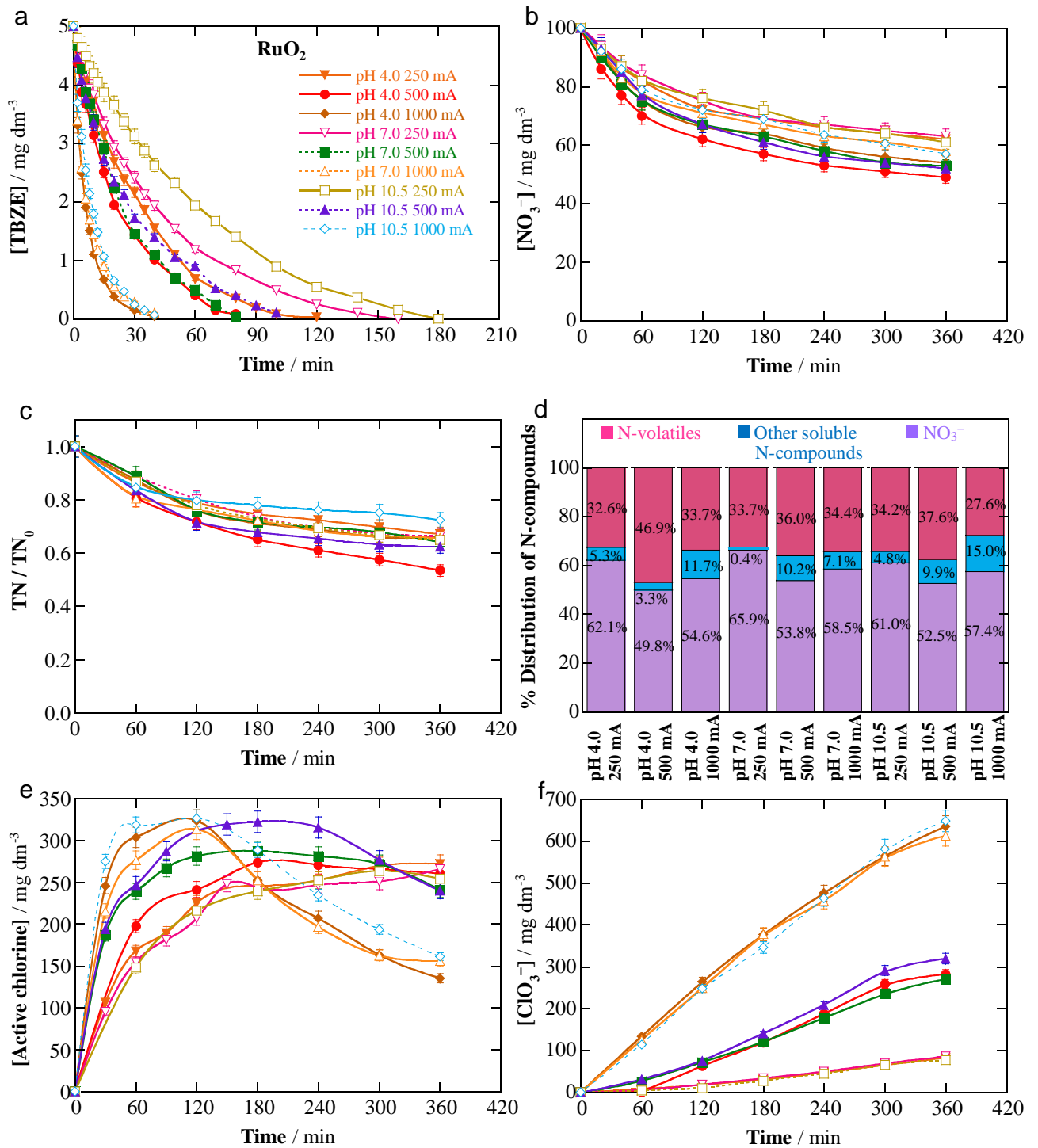
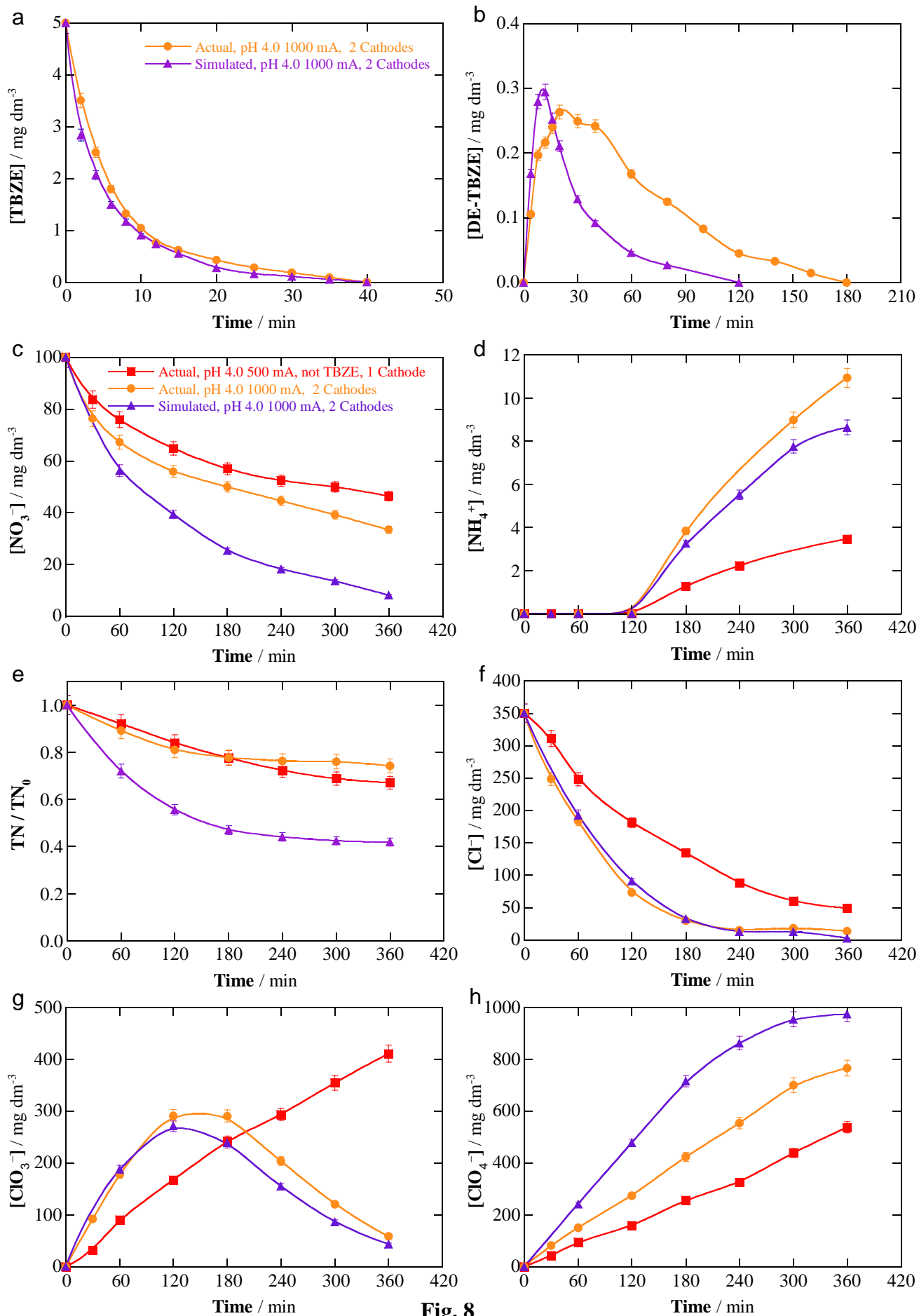


Fig. 6



**Fig. 7**



**Fig. 8**



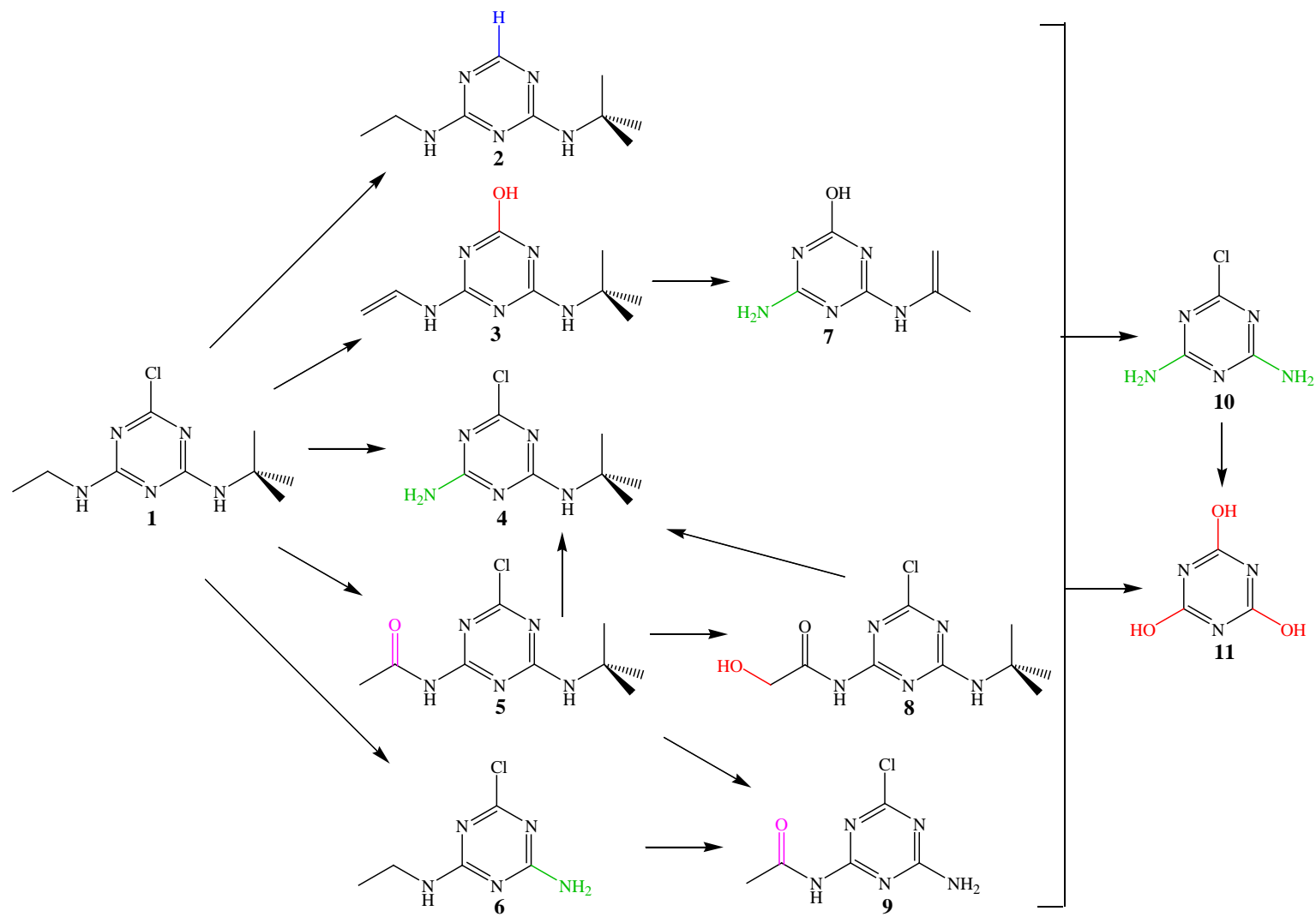


Fig. 9

**Table 1**

Physicochemical characteristics of the raw groundwater, the softened groundwater after conditioning at pH 4.00 and addition of 5 mg dm<sup>-3</sup> TBZE, the electrolyzed softened groundwater after 360 min of an EO/electrodenitrification treatment in an undivided stirred BDD/Fe tank reactor at  $I = 500$  mA and 25 °C, and the same final solution once post-treated with Purolite<sup>®</sup> A532E ion-exchange resin.

Parameter (units)	Raw groundwater	Softened groundwater	Electrolyzed groundwater	Post-treated groundwater
pH	7.19	4.00	10.20	8.31
Conductivity (mS cm <sup>-1</sup> )	1.72	1.93	1.90	2.02
TC (mg dm <sup>-3</sup> )	50.02	- <sup>a</sup>	- <sup>a</sup>	- <sup>a</sup>
TOC (mg dm <sup>-3</sup> )	1.30	3.74	2.43	2.22
TN (mg dm <sup>-3</sup> )	23.89	23.77	16.76	10.58
NO <sub>3</sub> <sup>-</sup> (mg dm <sup>-3</sup> )	101.32	99.76	33.43	5.26
NO <sub>2</sub> <sup>-</sup> (mg dm <sup>-3</sup> )	- <sup>b</sup>	- <sup>b</sup>	2.72	- <sup>b</sup>
Cl <sup>-</sup> (mg dm <sup>-3</sup> )	363.26	344.26	42.2	712.31
ClO <sub>3</sub> <sup>-</sup> (mg dm <sup>-3</sup> )	- <sup>b</sup>	- <sup>b</sup>	58.74	3.24
ClO <sub>4</sub> <sup>-</sup> (mg dm <sup>-3</sup> )	- <sup>b</sup>	- <sup>b</sup>	766.61	- <sup>b</sup>
SO <sub>4</sub> <sup>2-</sup> (mg dm <sup>-3</sup> )	77.52	357.21	358.56	56.91
Ca <sup>2+</sup> (mg dm <sup>-3</sup> )	99.59	0.87	0.84	1.31
Mg <sup>2+</sup> (mg dm <sup>-3</sup> )	26.57	0.55	- <sup>b</sup>	- <sup>b</sup>
K <sup>+</sup> (mg dm <sup>-3</sup> )	9.9	10.47	10.67	11.49
Na <sup>+</sup> (mg dm <sup>-3</sup> )	179.90	389.74	384.53	386.30

<sup>a</sup> Not measured. <sup>b</sup> Not found

**Table 2**

Pseudo-first-order rate constant for  $\text{NO}_3^-$ ,  $\text{Cl}^-$  and terbuthylazine decays, alongside the energy consumption at 360 min of electrolysis, for the treatment of  $500 \text{ cm}^3$  of simulated groundwater matrices and softened actual groundwater in the absence and presence of herbicide at different pH values and  $25^\circ\text{C}$ . The assays were made using undivided cells with a BDD or  $\text{RuO}_2$  anode and an Fe cathode.

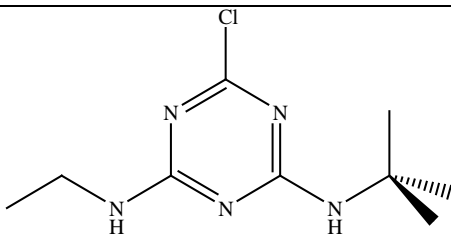
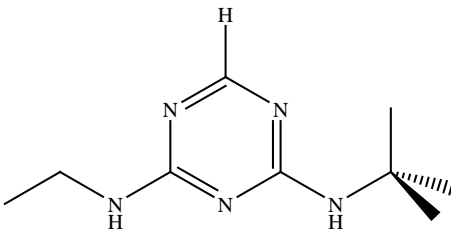
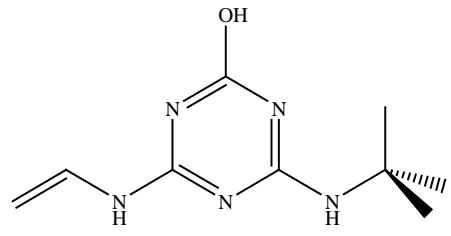
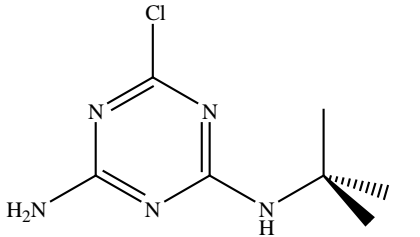
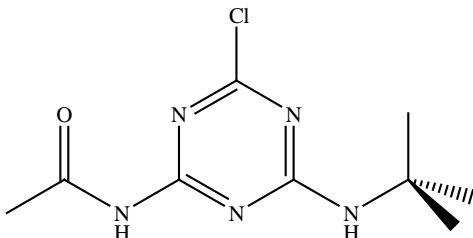
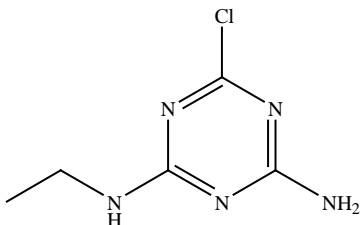
Anode	pH <sub>0</sub> (pH <sub>f</sub> )	<i>I</i> / mA	<i>E</i> <sub>cell</sub> / V	<i>k</i> ( $\text{NO}_3^-$ ) / $10^{-3} \text{ min}^{-1}$ ( <i>R</i> <sup>2</sup> )	<i>k</i> ( $\text{Cl}^-$ ) / $10^{-3} \text{ min}^{-1}$ ( <i>R</i> <sup>2</sup> )	<i>k</i> (TBZE) / $10^{-2} \text{ min}^{-1}$ ( <i>R</i> <sup>2</sup> )	EC / kWh $\text{m}^{-3}$
<i>Simulated groundwater (100 mg dm<sup>-3</sup> NO<sub>3</sub><sup>-</sup> + 7.6 mM SO<sub>4</sub><sup>2-</sup>)</i>							
BDD	4.0 (10.3)	500	8.4	4.7 (0.990)	-	-	50.4
	7.0 (10.7)	500	8.3	5.2 (0.988)	-	-	49.8
	10.5 (10.8)	500	7.5	4.6 (0.981)	-	-	45.0
RuO <sub>2</sub>	4.0 (10.1)	500	6.7	6.3 (0.987)	-	-	40.2
	7.0 (11.2)	500	6.5	2.5 (0.997)	-	-	39.0
	10.5 (10.0)	500	6.9	5.0 (0.993)	-	-	41.4
<i>Simulated groundwater (10 mM Cl<sup>-</sup> + 100 mg dm<sup>-3</sup> NO<sub>3</sub><sup>-</sup> + 0.8 mM SO<sub>4</sub><sup>2-</sup>)</i>							
BDD	4.0 (10.3)	250	5.4	3.3 (0.991)	3.4 (0.988)	-	16.2
	4.0 (10.2)	500	8.5	4.3 (0.980)	7.5 (0.994)	-	51.0
	7.0 (10.3)	500	8.6	3.9 (0.993)	5.1 (0.981)	-	51.6
	10.5 (10.4)	500	8.0	3.2 (0.980)	7.0 (0.986)	-	48.0
	4.0 (10.7)	1000	13.5	6.1 (0.988)	12.4 (0.993)	-	162.0
RuO <sub>2</sub>	4.0 (8.4)	500	7.5	2.8 (0.997)	1.6 (0.985)	-	45.0
	7.0 (9.8)	500	7.5	2.5 (0.995)	1.7 (0.980)	-	45.0
	10.5 (10.0)	500	7.3	1.8 (0.997)	1.5 (0.991)	-	43.8
<i>Simulated groundwater (5.0 mg dm<sup>-3</sup> TBZE + 10 mM SO<sub>4</sub><sup>2-</sup>)</i>							
BDD	4.0 (4.35)	500	8.3	-	-	9.0 (0.998)	49.8
<i>Simulated groundwater (5.0 mg dm<sup>-3</sup> TBZE + 100 mg dm<sup>-3</sup> NO<sub>3</sub><sup>-</sup> + 7.6 mM SO<sub>4</sub><sup>2-</sup>)</i>							
BDD	4.0 (9.3)	500	8.0	2.2 (0.981)	-	5.7 (0.988)	48.0
RuO <sub>2</sub>	4.0 (10.9)	500	7.5	6.5 (0.989)	-	0.63 (0.994)	45.0
<i>Simulated groundwater (5.0 mg dm<sup>-3</sup> TBZE + 10 mM Cl<sup>-</sup> + 100 mg dm<sup>-3</sup> NO<sub>3</sub><sup>-</sup> + 0.8 mM SO<sub>4</sub><sup>2-</sup>)</i>							
BDD	4.0 (10.6)	250	5.8	2.1 (0.984)	- <sup>a</sup>	4.5 (0.997)	17.4
	4.0 (9.9)	500	9.1	3.6 (0.988)	- <sup>a</sup>	9.9 (0.998)	54.6
	4.0 (10.4)	1000	14.7	4.3 (0.993)	- <sup>a</sup>	12.0 (0.993)	176.4
	7.0 (10.6)	250	6.1	2.5 (0.998)	- <sup>a</sup>	4.3 (0.991)	18.3

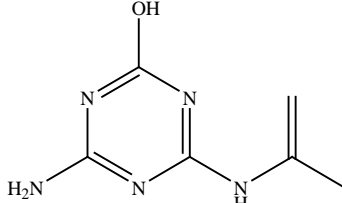
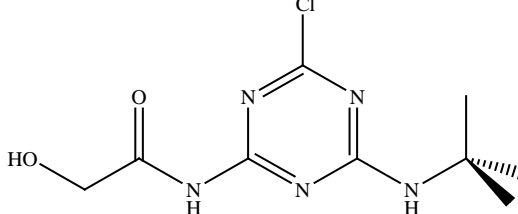
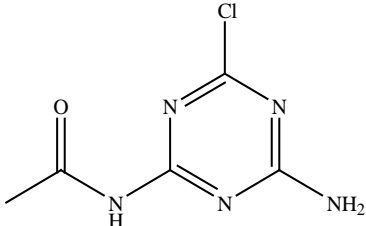
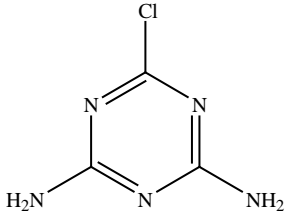
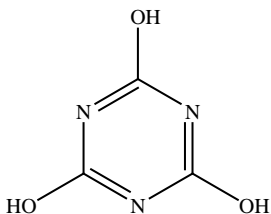
	7.0 (10.5)	500	10.4	3.3 (0.982)	- <sup>a</sup>	5.6 (0.991)	62.4
	7.0 (10.0)	1000	16.3	2.8 (0.980)	- <sup>a</sup>	7.2 (0.985)	185.6
	10.5 (9.8)	250	6.7	2.1 (0.983)	- <sup>a</sup>	3.6 (0.995)	20.1
	10.5 (10.4)	500	9.2	4.4 (0.981)	- <sup>a</sup>	5.2 (0.993)	55.2
	10.5 (10.0)	1000	14.2	3.6 (0.982)	- <sup>a</sup>	8.0 (0.995)	170.4
BDD <sup>b</sup>	4.0 (10.6)	1000	8.8	6.6 (0.993)	14.0 (0.990)	16.5 (0.982)	105.6
RuO <sub>2</sub>	4.0 (9.6)	250	4.4	3.3 (0.986)	- <sup>a</sup>	3.4 (0.988)	13.2
	4.0 (9.7)	500	8.0	5.9 (0.989)	- <sup>a</sup>	4.7 (0.980)	48.0
	4.0 (10.1)	1000	14.2	5.0 (0.991)	- <sup>a</sup>	11.1 (0.993)	170.4
	7.0 (9.8)	250	5.3	3.0 (0.981)	- <sup>a</sup>	2.4 (0.996)	15.4
	7.0 (9.8)	500	8.3	4.8 (0.995)	- <sup>a</sup>	4.1 (0.993)	49.8
	7.0 (9.3)	1000	14.1	4.4 (0.997)	- <sup>a</sup>	9.1 (0.991)	169.2
	10.5 (10.3)	250	4.9	3.3 (0.998)	- <sup>a</sup>	1.8 (0.991)	14.7
	10.5 (10.3)	500	8.9	4.4 (0.995)	- <sup>a</sup>	3.0 (0.992)	53.4
	10.5 (9.5)	1000	13.4	3.9 (0.998)	- <sup>a</sup>	9.8 (0.998)	160.8
<i>Softened actual groundwater</i>							
BDD <sup>c</sup>	4.0 (9.7)	500	7.1	- <sup>e</sup>	5.7 (0.996)	- <sup>a</sup>	42.6
BDD <sup>b,d</sup>	4.0 (10.2)	1000	8.9	- <sup>e</sup>	13.4 (0.997)	15.6 (0.997)	106.8

<sup>a</sup> Not determined. <sup>b</sup> 2 Fe cathodes. <sup>c</sup> Without and <sup>d</sup> with 5.0 mg dm<sup>-3</sup> TBZE. <sup>e</sup> Nonlinear correlation.

**Table 3**

Products identified by GC-MS after 60 min of EO/electrodenitrification of 500 cm<sup>3</sup> of solutions with 5.0 mg dm<sup>-3</sup> terbuthylazine in a simulated matrix at pH 4.0 and 25 °C using a BDD/Fe cell at 500 mA.

No.	Chemical name	Molecular structure	Column <sup>a</sup>	<i>t<sub>r</sub></i> / min	Fragments <sup>b</sup> <i>m/z</i>
1	Terbuthylazine (TBZE)		P <sup>c,d</sup> NP <sup>c,d</sup>	40.71 30.73	229 214 (- CH <sub>3</sub> ) 173 (- C(CH <sub>3</sub> ) <sub>3</sub> + H) 158 (173 - CH <sub>3</sub> )
2	<i>N</i> - <i>tert</i> -butyl- <i>N'</i> - [1,3,5]triazine-2,4- diamine <sup>a,b</sup>		P <sup>c</sup> NP <sup>c,d</sup>	33.93 26.92	195 180 (- CH <sub>3</sub> ) 139 (- (C(CH <sub>3</sub> ) <sub>3</sub> + H)) / - CH <sub>3</sub> - CH <sub>2</sub> -NH-C-)
3	4- <i>tert</i> buthylamino- 6-vinylamino- [1,3,5]triazine-2-ol		P <sup>d</sup> NP <sup>d</sup>	40.47 29.84	209 194 (- CH <sub>3</sub> ) / 152 (- C(CH <sub>3</sub> ) / 194 - C(CH <sub>3</sub> ) <sub>2</sub> ) 125 (152 - CH=CH <sub>2</sub> )
4	(Desethyl- terbuthylazine), <i>N</i> - <i>tert</i> -butyl-6- chloro- [1,3,5]triazine-2,4- diamine (DE-TBZE)		P <sup>c</sup>	43.98	201 186 (- (NH <sub>2</sub> + H)) 145 (- (C(CH <sub>3</sub> ) <sub>3</sub> + H)) 173 (- C(NH <sub>2</sub> )-) 138 (173 -Cl)
5	<i>N</i> -(4- <i>tert</i> - butylamino-6- chloro- [1,3,5]triazine-2- yl)-acetamide		P <sup>c</sup> NP <sup>d</sup>	45.31 33.23	243 228 (- CH <sub>3</sub> ) 200 (- (CO- CH <sub>3</sub> )) 186 (- C(CH <sub>3</sub> ) <sub>3</sub> )
6	6-chloro- <i>N</i> -ethyl- [1,3,5]triazine-2,4- diamine		P <sup>c,d</sup> NP <sup>c,d</sup>	47.42 28.36	173 158 (- (NH <sub>2</sub> + H)) / - CH <sub>3</sub> ) 145 (- (CH <sub>2</sub> - CH <sub>3</sub> + H)) 110 (145 -Cl)

7	4-amino-6-isopropenylamino-[1,3,5]triazine-2-ol		P <sup>d</sup>	36.56	167 152 (- CH <sub>3</sub> ) 111 (- NH-C(CH <sub>2</sub> )-CH <sub>3</sub> )
8	<i>N</i> -(4- <i>tert</i> -butylamino-6-chloro-[1,3,5]triazine-2-yl)-2-hydroxyacetamide		P <sup>c</sup>	42.60	259 185 (- NH-C(O)-CH <sub>2</sub> OH) 129(185 - (C(CH <sub>3</sub> ) <sub>3</sub> +H))
9	<i>N</i> -(4-amino-6-chloro-[1,3,5]triazine-2-yl)-acetamide		P <sup>c</sup>	45.48	187 172 (- CH <sub>3</sub> ) 145 (- (C(O)-CH <sub>3</sub> +H)) 110 (145 - Cl)
10	6-chloro-[1,3,5]triazine-2,4-diamine		P <sup>d</sup>	41.89	145
11	Cyanuric acid		P <sup>c</sup>	30.27	129 115 (- N-) 98 (115 - OH) 87 (129 - (N-C(OH)- + H)) 73 (87 - N-)

<sup>a</sup> P: polar column, NP: Nonpolar column. <sup>b</sup> The mass (*m*) of chlorinated fragments considered the isotope <sup>35</sup>Cl. <sup>c</sup> Medium: 100 mg dm<sup>-3</sup> NO<sub>3</sub><sup>-</sup> + 7.6 mM SO<sub>4</sub><sup>2-</sup>. <sup>d</sup> Medium: 10 mM Cl<sup>-</sup> + 100 mg dm<sup>-3</sup> NO<sub>3</sub><sup>-</sup> + 0.8 mM SO<sub>4</sub><sup>2-</sup>